Atmospheric Environment 134 (2016) 181–197

Contents lists available at ScienceDirect

Atmospheric Environment

journal homepage: www.elsevier.com/locate/atmosenv

Chemical characterization of freshly emitted particulate matter from aircraft exhaust using single particle mass spectrometry

Manuel Abegglen [a, *], B.T. Brem [b, c], M. Ellenrieder [d], L. Durdina [b, c], T. Rindlisbacher [e], J. Wang [b, c], U. Lohmann [a, **], B. Sierau [a]

[a] Institute for Atmospheric and Climate Science, ETH Zurich, Switzerland
[b] Laboratory for Advanced Analytical Technologies, Empa, Dübendorf, Switzerland
[c] Institute of Environmental Engineering, ETH Zurich, Zurich, Switzerland
[d] SR Technics, Zurich, Switzerland
[e] Swiss Federal Office of Civil Aviation, Bern, Switzerland

HIGHLIGHTS

- First PM aircraft exhaust measurements using single particle mass spectrometry.
- The majority of the investigated particles contained one or more metallic compound.
- The metals and the soot were found to be internally mixed in the emitted particles.
- Potential sources of the detected metals (fuel, oil and engine wear) were discussed.

ARTICLE INFO

Article history:
Received 17 December 2015
Received in revised form
26 March 2016
Accepted 29 March 2016
Available online 30 March 2016

Keywords:
Particulate matter
Aircraft emission
Soot
Metal tracers
Single particle mass spectrometry
Chemical characterization
A-PRIDE

ABSTRACT

Non-volatile aircraft engine emissions are an important anthropogenic source of soot particles in the upper troposphere and in the vicinity of airports. They influence climate and contribute to global warming. In addition, they impact air quality and thus human health and the environment. The chemical composition of non-volatile particulate matter emission from aircraft engines was investigated using single particle time-of-flight mass spectrometry. The exhaust from three different aircraft engines was sampled and analyzed. The soot particulate matter was sampled directly behind the turbine in a test cell at Zurich Airport. Single particle analyses will focus on metallic compounds. The particles analyzed herein represent a subset of the emissions composed of the largest particles with a mobility diameter >100 nm due to instrumental restrictions. A vast majority of the analyzed particles was shown to contain elemental carbon, and depending on the engine and the applied thrust the elemental carbon to total carbon ratio ranged from 83% to 99%. The detected metallic compounds were all internally mixed with the soot particles. The most abundant metals in the exhaust were Cr, Fe, Mo, Na, Ca and Al; V, Ba, Co, Cu, Ni, Pb, Mg, Mn, Si, Ti and Zr were also detected. We further investigated potential sources of the ATOFMS-detected metallic compounds using Inductively Coupled Plasma Mass Spectrometry. The potential sources considered were kerosene, engine lubrication oil and abrasion from engine wearing components. An unambiguous source apportionment was not possible because most metallic compounds were detected in several of the analyzed sources.

1. Introduction

The continuous increase of commercial air traffic has led to rising public awareness and concerns about the associated Particulate Matter (PM) emissions. The annual future growth rate is estimated to be 3.4–6.1% (ICAO, 2013) in terms of passenger revenue kilometers. The PM legislation regarding aircraft emission

* Corresponding author. ETH Zurich Institute for Atmospheric and Climate Science, CHN O 17.1, Universitätstrasse 16, 8092 Zurich, Switzerland.
** Corresponding author. ETH Zurich Institute for Atmospheric and Climate Science, CHN O 11, Universitätstrasse 16, 8092 Zurich, Switzerland.
E-mail addresses: amanuel@ethz.ch (M. Abegglen), ulrike.lohmann@env.ethz.ch (U. Lohmann).

http://dx.doi.org/10.1016/j.atmosenv.2016.03.051
1352-2310/

however, has been lagging behind general emission regulations from other combustion sources (e.g. road traffic). Up to now, the standard way to regulate PM emissions for aircraft engines manufactured after 1983 is to limit smoke number (ICAO, 2008). Smoke number is a unit derived from filter measurements using its change in reflectance after sampling a prescribed volume of exhaust. The smoke number standard is an exhaust plume non-visibility criteria. It is insufficient to assess particulate matter related air quality and climate impacts from aircraft engines. In the course of the recent development of an ICAO particulate matter certification standard for aircraft engines, the Aviation Particulate Regulatory Instrumentation Demonstration Experiment (A-PRIDE) campaigns were initiated. The A-PRIDE campaigns were conducted in the SR Technics facility at Zurich Airport in Switzerland. Previous studies from the A-PRIDE campaigns focused primarily on the physical characterization of the exhaust particles (Durdina et al., 2014; Abegglen et al., 2015) and evaluation of the sampling system in order to demonstrate its suitability for aircraft emission certification (Lobo et al., 2015). The used sampling system complies with the regulations on non-volatile aircraft engine emission certification documented in the Aerospace Information Report 6241 by the Society of Automotive Engineers (SAE, 2013). Additional information regarding the standard methods can be found in SAE (2004) and SAE (2010). Herein, we focus on the chemical characterization of PM in the aircraft engine exhaust. The presented measurements were mainly conducted during A-PRIDE 5 in 2013 investigating a very common in-production turbofan engine, using an Aerosol Time-of-Flight Mass Spectrometer (ATOFMS, TSI Model 3800-030). The ATOFMS allows to investigate the chemical composition of single particles, and the A-PRIDE campaigns offered a great and rare opportunity to sample and study unaltered combustion products from aircraft engines.

The emitted PM from aviation is of interest because it represents a unique anthropogenic source of soot particles in the upper troposphere and in the vicinity of airports. These particles alter the Earth's radiation budget in various ways depending on their physical and chemical properties. Based on findings presented in the special report on aviation and the global atmosphere (IPCC, 1999) and IPCC AR4 WG1 (IPCC, 2007), Lee et al. (2009) divided the climate effects from aircraft PM on climate into three radiative forcing components: soot aerosols, linear condensation trails (contrails), and induced cirrus cloudiness, which are all believed to result in a warming. In addition, the emitted particles could act as Ice Nucleating Particles (INP) and affect natural clouds.

Freshly emitted soot particles scatter and absorb solar radiation. Due to the chemical composition and microstructure of these particles, they primarily absorb solar radiation. A higher Elemental Carbon (EC) content enhances absorption of radiation whereas a lower EC content leads to an increase of the single scattering albedo (Qiu et al., 2014). The magnitude of the absorbed solar radiation strongly depends on particle size. Absorption coefficient calculations for a typical aircraft engine exhaust aerosol are given in Petzold and Schröder (1998). Linear contrails form just behind aircraft due the emission of heat and water vapor and formation depends on the ambient temperature and ambient air humidity as well as on the exhaust temperature and mixing processes after emission. The cooling of the exhaust stream causes water vapor to condense onto a fraction of the emitted particles and to freeze subsequently if the temperature is sufficiently low. Contrails cause a positive radiative forcing due to their occurrence at high altitude. Similarly to thin cirrus clouds, they reflect little incoming solar radiation back to space but absorb terrestrial infrared radiation. Their global coverage for the year 2006 was detected via satellite to be 0.07% (Duda et al., 2013). Research on occurrence and formation of contrails dates back almost 100 years and is well summarized in the review article from Schumann (1996). If the ambient air is supersaturated with respect to ice, the formed ice particles continue to grow and can form a persistent contrail. The largest radiative forcing arises from the induced cirrus caused by the possible evolution of linear contrails into persisting cirrus clouds (Burkhardt and Kärcher, 2011). These spreading cirrus clouds can become undistinguishable from naturally (e.g. synoptically or orographically) evolved cirrus clouds. With a confidence of 90%, the aviation-induced radiative forcing in 2005 was estimated to be in the range 23–87 mW/m^2 without aviation-induced cirrus and 38–139 mW/m^2 including cirrus cloud formation, corresponding to a 4.9% (2–14%) contribution to the anthropogenic forcing (Lee et al., 2009).

Moreover, it has been found that some fraction of carbon-containing particles are efficient INPs (Cozic et al., 2008). Thus, aircraft emissions can lead to regionally increased INP concentration affecting natural cirrus clouds even in the absence of contrail formation (Kärcher et al., 2007), including changes in optical properties and delays of freezing onsets (Burkhardt and Kärcher, 2011). This is explained by additional heterogeneous INP inhibiting the homogeneous freezing of the background aerosol particles, due to the decreased water content available. The magnitude of this effect remains uncertain because it depends heavily on the ice-nucleating efficiency of the emitted soot particles and of the background aerosol particles which are not yet completely understood (Zhou and Penner, 2014). A study performed by Cziczo et al. (2013) tackling the properties of INP in the upper troposphere showed that a dominant fraction of Ice Residuals (IR) collected in cirrus clouds contain metal compounds such as sodium, potassium, copper, lead and iron. These compounds have also been found in aircraft emissions by sampling the exhaust (Agrawal et al., 2008). Also, Cziczo et al. (2009) showed that lead-containing mineral dust particles are efficient INP, as a consequence, lead- or metal-containing particles might increase the INP number in the atmosphere. Thus, a thorough chemical characterization of single particles from fresh aircraft PM emissions provides information to study the link between aircraft emissions and ice formation processes in the atmosphere.

The radiative and ice-nucleating properties change over time as the soot particles undergo aging by the uptake of water and/or secondary volatile species and oxidation. These processes are partly influenced by the particle's initial composition (Rudich et al., 2007). The Organic Carbon (OC) components on the particle surface were found to be important for the aging process of soot and may even alter the Cloud Condensation Nuclei (CCN) or INP activity when they are oxidized by O_2 under solar radiation and turn into soluble organics (Han et al., 2012).

Aviation PM emissions are also of importance as PM in general is known to cause adverse health issues. The emitted particles have been shown to be small with a geometric mean diameter well below 100 nm (Lobo et al., 2007; Kinsey et al., 2010; Abegglen et al., 2015) and therefore fall mainly into the particle class described as ultrafine PM ($PM_{0.1}$). Ultrafine particles can penetrate deeper into the human respiratory system and are less likely to be removed than larger particles and may be able to enter the blood stream (Terzano et al., 2010). Health effects in general seem to be more associated with Black Carbon emission (BC) than with PM_{10} or $PM_{2.5}$ alone (Janssen et al., 2012), but it was not possible to show that BC directly is a toxic component. Janssen et al. (2012) therefore summarizes that BC probably acts as a carrier for toxic substances. This supports findings from an earlier study showing that particles containing metals such as vanadium, iron, copper and nickel can cause epithelial injuries (Pagan et al., 2003). It seems intuitive that the largest respiratory health effects caused by aircraft emissions are found in the vicinity of airports (Keuken et al., 2015), especially

for workers at airports (Touri et al., 2013). However, emissions can cause health effects not only in the vicinity of airports but also on larger spatial scales (Yim et al., 2015).

Earlier studies on PM aircraft emissions focused primarily on the particle size and concentration in proportion to the thrust applied to the engine (Petzold and Schröder, 1998; Rogers et al., 2005; Corporan et al., 2008; Herndon et al., 2008; Onasch et al., 2009). Investigations on the composition in terms of organic content have also been performed (Onasch et al., 2009; Timko et al., 2010; Lobo et al., 2015). Literature on the investigations of PM aircraft emissions with respect to the chemical composition is also available. Fordyce and Sheibley (1975) used trace element content analysis from jet fuel to estimate corresponding concentrations in typical exhaust gas. Kinsey et al. (2011) sampled exhaust plumes from commercial aircraft at a distance of ~30 m behind the engine using optical instruments to provide data on BC concentrations and gravimetric analysis of filters to investigate the elemental composition quantitatively. Agrawal et al. (2008) conducted measurements on commercial aircrafts and presented emission indices of PM, elemental and organic carbon as well as of metallic compounds detected in the exhaust. Vander Wal and Bryg (2014) performed X-ray photoelectron spectroscopy to investigate jet exhaust particles from different aircraft and found varying amounts of N, S, Na, Ca, Zn, Ba, Sn, Cr and Al. However, the investigation of aircraft PM emission in terms of chemical characterization from single particles is still in an early stage and only few studies exist. Demirdjian et al. (2007) sampled soot particles emitted by an aircraft gas turbine engine directly behind the engine duct in order to investigate the composition of soot agglomerates. The sample was then deposited on copper microgrids and analyzed. They have found impurities of Fe, O, S, K and Mn. Mazaheri et al. (2013) collected PM_1 samples on filters and membrane grids 200 m from an airfield runway in order to perform elemental analysis on discrete particles using energy dispersive X-ray spectroscopy. They found C, O, S, Cl, Na, Al, Si, Ca, Ti, Cr, Fe, Co, Ni, Cu, Zn, and Pb but attributed them not only to engine exhaust but to a diverse range of sources such as tire wear, dust and automotive traffic. Especially studies on fresh aircraft exhaust sampled directly behind the engine remain scarce and no study exists to our knowledge that investigates the chemical composition of freshly emitted aircraft exhaust particles using in-situ single particle mass spectrometry. Our study focuses on a general chemical characterization of single particles sampled directly behind the engine with emphasis on metallic compounds in the particles.

2. Methods

2.1. Measurement campaigns and location

The majority of the measurements presented herein were conducted during the dedicated Aviation – Particle Regulatory Instrument Demonstration Experiment 5 (A-PRIDE 5) campaign in July and August 2013. Additional data was collected during piggyback measurements in Mai 2015. The campaigns took place at the airport Zurich where the measurements were conducted in a test cell of SR Technics. The facility is located in the southeastern corner of the airport area. A tram route and a road are going by in the east of the test cell at a distance of <50 m and a freeway at ~100 m.

The particle emissions of three in-production, high-bypass turbofan engines were investigated. All of the engines are widely used in the current aircraft fleet. Engine 1 and 2 were core-flow single annular combustor types with rated outputs in the range of 120 kN, here referred to as “Turbofan 1 and 2”, respectively. Engine 3, here referred to as “Mixed-Flow Turbofan” utilized also a single annular combustor with rated output of ~150 kN, but its exhaust is diluted with its bypass air at a ratio of approximately 6:1. All engines were fueled with standard Jet A-1 fuel. The applied engine thrust was set using the combustor inlet temperature, which in turn was used to predict the static thrust the engine would produce at 1013 hPa ambient pressure and 15 °C. Thus, this predicted thrust reported herein can exceed 100%.

2.2. Experimental set-up

The emitted particles were sampled by a probe oriented parallel to the exhaust flow (Fig. 1). The sampling probe was positioned at a distance of ~0.7 m behind the engine duct, guiding the emissions through an 8 mm inner diameter stainless steel pipe heated to 160 °C to the sampling system. A tee was used to split the sample into two main measurement lines referred to as the PM line and the Annex 16 line. The PM line was mainly used for measurements of non-volatile PM number and mass whereas the Annex 16 line was mainly used to measure gaseous species. Both lines were conductive PTFE and ~25 m in length before leading to the measuring instruments. Both lines were heated in order to prevent condensation of volatile species onto the sampled particles. The PM line was diluted by a factor of ~8–12 with synthetic air (grade 5.0) using a Dekati ejector dilutor (Dekati, Model DI 1000, Dekati Ltd., Kangasala, Finland). At the dilution point, the PM line temperature was reduced from 160 °C to 60 °C. This 60 °C line was used for the PM instrumentation and the ATOFMS. The undiluted Annex 16 line was maintained at 160 °C leading to the Annex 16 gaseous analyzers. A tee at the end of this line was used to guide the sample through a 60 °C heated line to a Nafion (Perma Pure, Model PD-100T-24 (MSS), Perma Pure LLC, Toms River, USA) dryer to the ancillary Annex 16 instruments and a Scanning Mobility Particle Sizer (SMPS, TSI, Model 3936, TSI Inc., St. Paul, USA) system. See Lobo et al. (2015) for a more detailed overview of the additional instruments and results from this experimental set-up.

2.3. Instruments

2.3.1. Aerosol time-of-flight mass spectrometer

An Aerosol Time-of-Flight Mass Spectrometer (ATOFMS, TSI Model 3800-030) was used to investigate the single particle chemical composition of non-volatile fresh emissions from aircraft engines. The ATOFMS is a mass spectrometer that measures the chemical composition of single particles and their vacuum aerodynamic diameter (d_{va}) (Gard et al., 1997) and has the capability to resolve refractory material such as EC as well as metallic compounds. Each mass spectra obtained allows the chemical analysis of this particle.

The ATOFMS works at low pressures which draws the sample flow into the instrument. It consists of three main regions with decreasing working pressures: 1) the particle sampling region (~270 Pa), 2) the particle sizing region (~10^{-3} Pa), and 3) the mass spectrometry region (~10^{-6} Pa). The sample flow rate into the instrument was 0.1 l/min, set by a critical orifice. A backup flow between 1 l/min and 3 l/min (depending on the flow needed by other instruments) was used to shorten the response time. Downstream of the critical orifice, the particles pass through an Aerodynamic Focusing Lens (AFL) that aligns the particles into a narrow beam and then into the sampling region. For this study, an AFL optimized for an aerodynamic particle size range from 30 nm to 300 nm was used (TSI, 2004). Once the particles are in the sizing region, they accelerate due to the pressure drop depending on their size and are detected by two consecutive continuous, orthogonally oriented wave diode-pumped lasers ($\lambda = 532$ nm). The time they need to travel between the sizing lasers is used to determine their aerodynamic size and to trigger the ionization laser in the following.

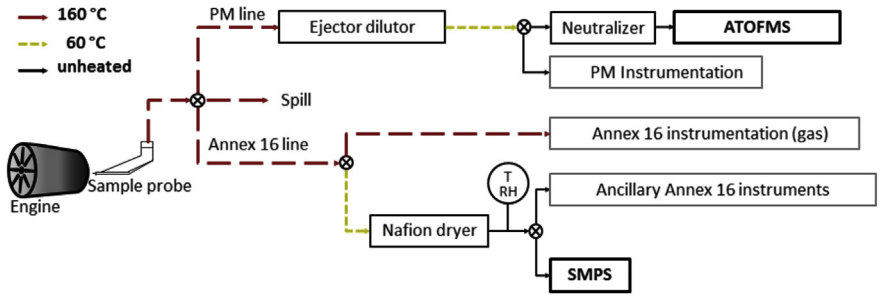

Fig. 1. Simplified schematic of the experimental set-up.

The particles then enter the mass spectrometry region where the particles are ionized by the ionization laser (Nd:YAG, $\lambda = 266$ nm), set to an energy of ~1 mJ/pulse. If the particle is hit by the ionization laser, it gets ablated and ionized, resulting in ions and molecules, both positive and negative. They are then separated according to their mass-to-charge ratio (m/z) by their mass-dependent acceleration in positive and negative electromagnetic fields in the flight tubes. The time (of flight) the individual constituents need to travel through the electromagnetic fields until they reach detector plates is recorded and converted into m/z values. The output is a positive and negative mass spectra for each ionized particle, revealing its aerodynamic size and chemical composition.

Before the particles entered the ATOFMS they were treated with a 210^{Po} neutralizer in order to minimize their electric charge increasing the hit rate (fraction of sized/registered particles that are ionized). This is because electrostatic forces can cause deviation of the particle's trajectory within the instrument.

The ATOFMS data itself is not quantitative because of several reasons. For example, the coating of a particle with secondary species was shown to decrease the ionization efficiency resulting in changes in the measured ion peak areas (Hatch et al., 2014). Moreover, different chemical species in the same particle can influence each other's ionization efficiencies due to the so-called matrix effects (Liu et al., 2000). Nevertheless, analysis of spectra from the same particle type using relative peak areas can reduce matrix effects to a certain extent because of lower spectrum to spectrum variability (Gross et al., 2000). Thus, average relative intensities from a large number of similar particles can be used to gain some information on relative differences in the mass of compounds in the particle when comparing different conditions.

2.3.2. Inductively coupled plasma mass spectrometry

Inductively Coupled Plasma Mass Spectrometry (ICP-MS) was used to analyze samples from fuel, lubrication oil and wearing from engine. Fuel and oil were analyzed using an ELAN 6100 (Perkin Elmer, Canada) whereas the sample from engine wear was analyzed using an ELAN 6100DRC^{+} (Perkin Elmer, Canada). ICP-MS is an offline method often used to measure metals from a bulk sample. It is very sensitive to the concentration of the analyzed compounds which can be as low as one part in 10^{-15}. It uses argon treated with a high frequency current in order to heat it up to ~10,000 K, turning the argon into a plasma. The sample is introduced with argon as carrier gas into the argon plasma where it is vaporized, atomized and ionized (Gross, 2011). The resulting ions are accelerated by an electromagnetic field and subsequently registered by detectors, and quantification is achieved by comparison with certified reference materials.

2.4. Data analysis

2.4.1. Identification of particle types and components

The mass spectra were analyzed using MS-Analyze and ENCHILADA (Environmental Chemistry through Intelligent Atmospheric Data Analysis) (Gross et al., 2010), two software programs designed to analyze ATOFMS data. This allowed further size resolved analysis of the particles or subclasses of particles using queries. Queries allow the identification of the compounds of particles by searching for the corresponding m/z values.

ENCHILADA was used for a cluster analysis of the analyzed particles. It groups similar spectra into clusters using different clustering algorithms (Giorio et al., 2012). Each resulting cluster is representative for a particle type that shows specific m/z values and ratios of intensities. This study used k-means, a clustering algorithm that allows to identify and define an adequate number of clusters. This method was used because only a small number of clusters were expected due to the high resemblance of the spectra. Similar clusters were manually merged together. The data presented in this study were analyzed with respect to engine thrust if enough data was obtained, i.e. the A-PRIDE 5 measurements. The particles were characterized with emphasis on the occurrence of metallic compounds. If interference with other peaks from other ions was observed, peaks from isotopes of the metallic compounds were used to discriminate.

Elemental Carbon to Total Carbon ratios (EC/TC) were derived from ATOFMS data adopting a method using the sum of relative peak areas associated with EC and TC presented by Ferge et al. (2006). TC is defined as the sum of Organic Carbon and EC. After subtracting peaks from known inorganic compounds from the average spectrum, TC was calculated by adding up all remaining peak areas. The list of inorganic compounds from Ferge et al. (2006) was modified by adding the metallic compounds found during our analysis. It is still possible that certain inorganic species were missed and not subtracted from the average spectra. However, none of the relevant remaining peaks was assigned to a known inorganic compound. EC was calculated from the average spectrum by adding up all peak areas at m/z $12i$, $12i + 1$, $12i + 2$ and $12i + 3$ (with $i = 1, 2$, etc.). The ratio of the obtained peak areas for EC and TC then yielded the presented EC/TC values. In this study from Ferge et al. (2006), the described method above was found to agree with a standardized thermo-optical approach using the NIOSH 5040 (Birch, 2002) method and a thermo-coulometric method, especially for samples with low inorganic content. Additionally, the particles were classified into 'EC' and 'ECOC' using criteria such that the 'EC' class composed particles with no OC whereas the 'ECOC' class composed particles showing both EC and OC signals. This was done by applying an "exclusive" classification query on the obtained positive spectra in MS-Analyze. This means, if particles are sorted into the first class for which they meet the prescribed requirements, they are then excluded from further classification. The

first class comprised the 'EC' particles. In order to define the 'ECOC' class, two additional classes, 'EC + K' and 'K noEC noOC', had to be defined and classified in advance because of the ambiguous association of the m/z +39 peak with organic compounds and potassium. This excludes the possibility of having particles in the 'ECOC' class that contain EC and potassium and no OC. The first additional class labelled as 'EC + K' was defined to show a peak at m/z +39 and the EC peaks. The second one labelled as 'K noEC noOC' was defined to show solely m/z +39 while not showing the other peaks associated with OC. Note that the presence of EC in the 'K noEC noOC' class is excluded due to the previous classification. Eventually, the 'ECOC' class was defined to consist of the remaining particles showing any combination of the OC and EC markers.

2.4.2. Particle size analysis

The vacuum aerodynamic diameter (d_{va}) of the analyzed aircraft exhaust particles was measured by the ATOFMS. Note that the ATOFMS was not used to determine the size distribution that is representative for the aircraft PM emission. d_{va} was converted into electrical mobility diameter (d_m) in order to compare d_{va} to continuous size measurements performed by a Scanning Mobility Particle Sizer (SMPS, TSI, Model 3936, TSI Inc., St. Paul, USA) system, which measures d_m. The calculation was done using equation [50] in DeCarlo et al. (2004):

$$d_{va} = \frac{\rho_p}{\rho_0} \frac{d_m}{\chi_v^{3/2}} \quad (1)$$

ρ_p and ρ_0 are the particle density and unit density respectively and χ_v is the dynamic shape factor in the vacuum or free molecular regime. ρ_p was assumed to be equal to the particle material density of soot. This holds for aggregates with no internal voids such as freshly evolved unaltered soot particles, and is supported by TEM pictures from aircraft soot (Liati et al., 2014; Boies et al., 2015). A value for ρ_p of 1.87 g/cm^3 as estimated from our previous effective density measurement on aircraft exhaust (Abegglen et al., 2015) was assumed. For comparison, other reported values of ρ_p range from 1.7 ± 0.7 g/cm^3 for non-volatile components of diesel soot (Park et al., 2004) up to 2.03 g/cm^3 (Braun et al., 2004) also for diesel soot. χ_v was calculated using equations [2.1] and [2.2] as described in Shapiro et al. (2012) with the information on particle mass and d_m also measured during A-PRIDE 5. Because the mass of a particle with a certain size additionally depends on engine thrust the mass was averaged over the measured thrusts. The value of χ_v is size-dependent and was calculated using a power law fit taking into account values obtained at different d_m. Additionally, the SMPS number size distributions combined with the thrust-dependent mass-size relationships presented in Abegglen et al. (2015) were used to infer mass size distributions.

3. Results and discussion

This chapter first gives an overview on the size of the investigated particles from aircraft engine exhaust. Information on the chemical composition of the identified particle types is provided, followed by EC to TC ratios determined from ATOFMS data. Lastly, the occurrence of metal compounds detected in the particles is presented and potential sources thereof are discussed. The latter is supported by ICP-MS analyses of the most likely sources that are engine jet fuel, lubrication oil and engine wear.

During the A-PRIDE 5 campaign, the ATOFMS was not able to record both the positive and the negative ion spectra because of instrumental restrictions. Thus, the vast majority of the data consists of positive spectra. It was possible to measure negative spectra during the last two days of the campaign, by switching the polarities of the high voltages applied to the flight tubes of the ATOFMS.

3.1. Size of investigated particles

The upper panel of Fig. 2 depicts the averaged thrust dependent SMPS measured size distributions shown as the particle mobility diameter emitted by Turbofan 1, collected via both, the PM line and the Annex 16 line. The middle panel shows the corresponding mass size distributions for 30%, 65% and 100% engine thrust. The lower panel shows the particle mobility diameter, calculated from the measured aerodynamic size as explained in Section 2.4.2, of the hit (i.e. chemically analyzed) particles by the ATOFMS during A-PRIDE 5. It can be seen that the ATOFMS measures the right hand tail of the number and mass size distributions as shown in the upper and middle panel, respectively. This is because the ATOFMS cannot size and analyze particles down to the mobility size of the majority of the emitted particles.

The mode of the SMPS number size distribution lies between 20 nm and 50 nm. By extrapolating the data assuming a log-normal distribution, the measured mobility size ranges from <10 nm to ~600 nm. The mobility size distribution of particles that were hit by the ATOFMS, however, shows a mode at ~400 nm and ranges from ~100 nm to ~700 nm. For the mass size distribution, the difference between the SMPS size distribution and the ATOMFS data is smaller increasing the overlap. The exact distributions of the hit particles remains unknown because the material density was assumed, and if it was higher, then the values calculated for d_m would be lower. Nevertheless, the size distributions would still differ in their modes. Although no differences in the chemical composition of the investigated particles were observed within the investigated size-range, our results cannot be reliably extrapolated towards smaller particles. Thus, the results presented in the following are only representative for the largest particles in the exhaust.

Experimental studies on the ice nucleating ability of soot showed that larger particles generally are more efficient INP than smaller ones (DeMott, 1990; Diehl and Mitra, 1998). Thus, assuming that particles emitted by aircraft engines can act as INP, their efficiency probably also increases with increasing particle size. Because we sampled the largest particles with the ATOFMS, they can be considered the fraction that is likely to be the most important regarding the contribution of aircraft emissions to INP.

3.2. Particle types

The particle types identified from the ATOFMS measured spectra through cluster analysis are presented in this section. Data from particles emitted by the three investigated engine types and the test cell background measurements are discussed.

3.2.1. Overview and comparison of the identified particle types

The particle types identified are summarized in Fig. 3 where the number in parentheses is the cluster number according to their source as described in detail in the following sections. The majority of the particle types identified for the aircraft engines showed a clear EC signal in their spectra. Only small differences were recognized between clusters (1), (3) and (5) from Turbofan 2 and clusters (1) and (3) from the Mixed-Flow Turbofan. They are similar to the EC-Na-metal particle type (cluster 1) presented for Turbofan 1 with respect to the positive ion spectra. Also, the common particles types from Turbofan 1 and the Mixed-Flow Turbofan were similar in terms of number fractions. Together, these particle types made up more than 75% of the measured particles for both engines. These engines mainly differed from Turbofan 1 because the metal-N particle type was not observed. However, this is probably due to

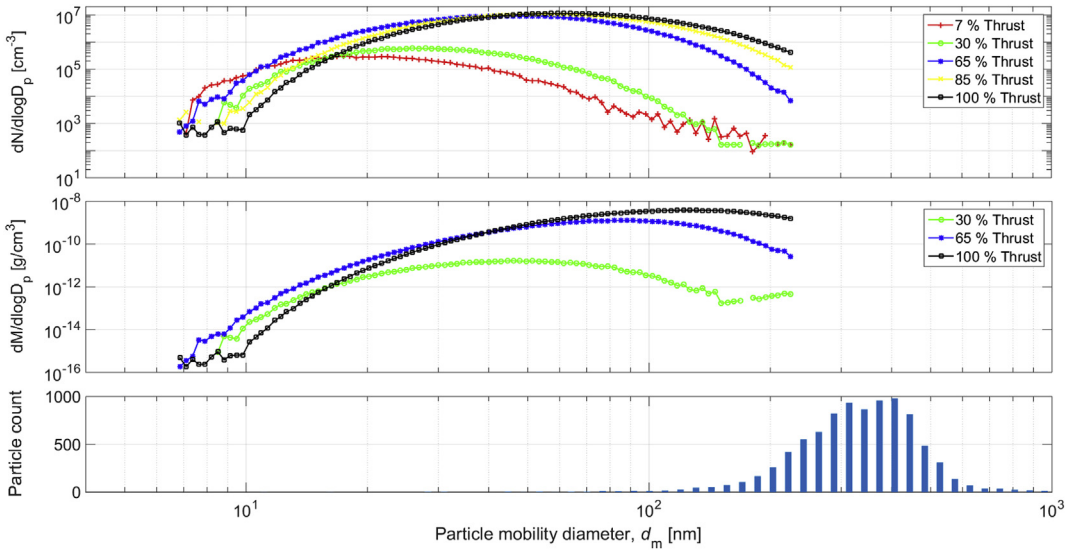

Fig. 2. SMPS measured number size (top) and inferred mass size (middle) distributions on the sampling line and the calculated mobility size of the particles chemically analyzed by the ATOFMS (bottom).

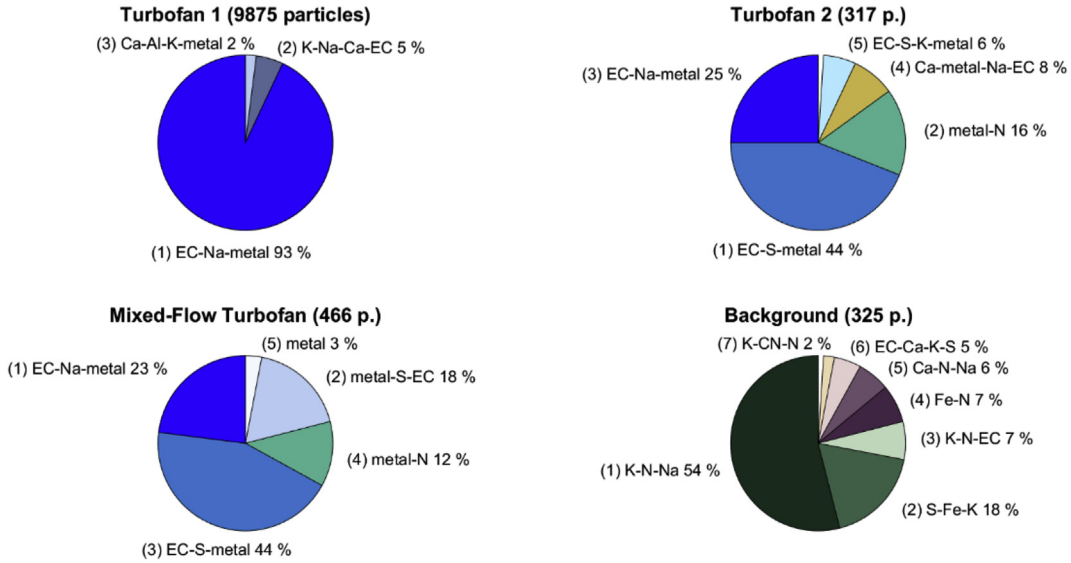

Fig. 3. Major particle types of the investigated aircraft engines and from the ambient background aerosol. The number in parentheses is the cluster number as described in the corresponding chapter.

missing the negative spectra.

The analysis of the ambient particles revealed that they do not resemble the exhaust particles sampled during engine runs. None of the particle types identified for ambient background aerosol were found in the aircraft exhaust, and only ~12% of the background particles depicted a clear EC pattern in both the positive and the negative spectrum. These particles were assumed to be remainders from previous engine tests or from sources in the vicinity such as landing and starting aircraft or cars. Most similarities exist between the K–N-EC (cluster 3) from the ambient background particles and the EC-Na-metal particle type from the engines, though the K–N-EC particle type clearly differs by the presence of nitrate and markers for organics. Nitrate however, is found in the metal-N particle type from the aircraft engines. As all ambient particle types contained nitrate, it is possible that nitrate from ambient aerosol is partly responsible for the nitrate detected in the particles emitted by the engines. The opposite is the case for the metallic compounds, especially aluminium, magnesium, vanadium, chromium, iron, manganese, molybdenum and barium. These are detected in most particle types of the engine emissions but only in clusters 2 and 4 from the ambient background particles.

Because of the different particle types detected in the exhaust and in the background, we assume that the background particles did not influence our exhaust measurements. In a similar way, we assume that the engine emissions from the engines have influenced the ambient background particles in terms of metallic compounds to some extent. Moreover, most metal compounds do not vaporize in the engine combustor according to their boiling points that exceed the maximum combustor temperature. Thus, the redistribution of the metal compounds from ambient particles onto the soot particles in the aircraft engine could only happen by coagulation. However, this would require the metallic compounds to be

externally mixed in the ambient aerosol and the cluster analysis showed that this was not case. Possible exceptions are calcium, sodium, and magnesium that have boiling points below the temperature in the engine potentially allowing their vaporization within the combustor. Calcium and sodium can both be abundant in ambient atmospheric aerosol and were also detected in our background measurements. So they can possibly be vaporized and redistributed via condensation onto the soot particles within the engine. However, considering the large difference in particle concentration between ambient air and exhaust their influence is thought to be minor.

3.2.2. Turbofan 1

For the spectra recorded during A-PRIDE 5 the clustering and the subsequent interpretation of the particle types were affected by the lack of negative mass spectra. In total 9875 positive spectra were obtained. The analysis of the mass spectra obtained from particles emitted yielded six clusters.

The mass spectra of the three major clusters (Fig. 4) represent >99% of the particles, the most prominent of which comprised ~93% of all chemically analyzed particles. They were classified as: (1) **EC-Na-metal** particles with a strong EC signature (m/z +12, +24, +36, +48, +60, +72, +84) and small peaks of inorganic compounds from sodium (m/z +23) and metals such as chromium (m/z +52) and iron (m/z +56). A small hydrocarbon peak (m/z +37 (C_3H)) indicates the presence of organic carbon (Spencer and Prather, 2006). The **K**–**Na**–**Ca-EC** particle type (2) has a dominant potassium signal (m/z +39, +41) and a sodium peak while including the EC pattern. This cluster comprises ~5% of the particles. The **Ca**–**Al**–**K-metal** particle type (3) comprises ~2% of the particles. It is dominated by a calcium peak at m/z +40 followed by an aluminium peak at m/z +27, a potassium and an iron peak. The peak at m/z +27 could also be attributed to organic carbon e.g. C_2H_3 (Silva and Prather, 2000; Pastor et al., 2003). However, from our EC/TC determination (see 3.3) and the fact that other possible markers of OC such as m/z +29, 37, 43, 51 and 63 (Spencer and Prather, 2006) are very weak, we assume the influence of OC to be smaller than from aluminium. The peak at m/z +56 is probably a mixture of Fe and CaO because of the small peak at m/z +57 that indicates the presence of CaOH. The three remaining clusters comprised 16 or less particles each and showed mainly one single peak at m/z +41 or +42 or +43. As a consequence, these clusters were assigned as unclassified.

By switching the polarities of the ATOFMS' flight tubes, we were able to analyze negatively charged ions and constituents, though the small number of spectra meant a cluster analysis was not meaningful. Instead, the average spectrum of the negative ions is presented in Fig. 5. Although it cannot be used to identify the individual particle types, it provides insight into most abundant chemical compounds of the analyzed particles. The average spectrum in terms of relative peak area mainly shows the presence of EC (peaks at m/z +12, +24, +36, etc.) and a prominent sulfate signal (m/z +97) which is a typical marker for sulfuric acid. The average negative spectrum agrees with the positive ions that also indicate a prevailing presence of EC.

Because all three major positive ion clusters indicated the presence of EC, we conclude that the detected inorganic and metallic compounds were all internally mixed with soot particles. This is also supported by the average negative spectrum and the fact that only 2.5% of the spectra did not show at least one peak associated with EC. Considering that some fraction of soot can effectively act as INP (Cozic et al., 2008) and that a dominant fraction of ice residuals in cirrus clouds contain metal compounds (Agrawal et al., 2008) the presented findings support the assumption that aircraft engine emissions can act as INP.

3.2.3. Turbofan 2

The cluster analysis resulted in nine clusters, of which five were considered to represent the main particle types (Fig. 6). Although the total number of spectra recorded was only 317, we still discuss the similarities to the particles sampled from Turbofan 1.

The **EC-S-metal** (1) was the most abundant particle type (~44%). Besides the very prominent sulfate ion peak at m/z −97 and the EC pattern, this cluster also shows the presence of metal compounds such as aluminium (m/z +27), chromium (m/z +52), iron (m/z +56) and molybdenum (m/z +92 − +100). The **metal-N** particle type (2) is made up from ~16% of the particles, and shows mainly metal compounds with the most pronounced peaks arising from magnesium (m/z +24 − +26), iron, barium (m/z +138) and calcium (m/z +40). Magnesium was identified due to the absence of other EC peaks and the matching isotopic ratio. Nitrate was identified by the peak at m/z −46. Here, the EC pattern is only present in the negative spectrum. The **EC-Na-metal** (3) particle type comprises ~25% of the particles, and is similar to cluster (1). However, this cluster includes a more intense sodium ion peak at m/z +23 and a lower intensity of the sulfate peak thus the negative EC pattern is relatively more pronounced. The **Ca-metal-Na-EC** particle type (4) shows combined features of EC, metal compounds and sodium. This cluster comprises ~8% of all particles, and contrary to the other clusters it shows strong signals of both barium and barium oxide. The peak at m/z −95 assigned to CH_3SO_3 is ambiguous due to the absence of other peaks from sulfates. Also, this peak has not been observed in other clusters. The peak at m/z −95 could potentially be associated with PO_4 or $NaCl_2$, however both are unlikely. The presence of phosphate is implausible because no peaks from PO_2 and PO_3 at m/z −63 and −79 were detected. For $NaCl_2$, an additional peak from its isotopes at m/z −93 would be expected. The **EC-S-K-metal** particle type (5) comprises ~6% of the particles. This cluster has very similar features to cluster (1) and (3), despite its dominant sulfate peak at m/z −96 instead at m/z −97. The spectra of the remaining four clusters make up ~1% of the total. These clusters all showed peaks associated with EC except for one. This cluster only contained one spectra with a major peak at m/z +90 potentially from zirconium and a peak at m/z −17 (OH).

3.2.4. Mixed-flow turbofan

The cluster analysis of the spectra obtained from the particles emitted by the Mixed-Flow Turbofan yielded six clusters, of which three were already identified for Turbofan 2. One cluster comprised only one particle. The word *cluster* might be not appropriate as it is actually only one particle. Nevertheless, we decided to call it a cluster for consistency and report it for the sake of completeness. The two clusters not identified for Turbofan 2, the metal-S-EC cluster (2) and the metal cluster (5), are depicted in Fig. 7. The total number of particles chemically analyzed from this engine was 466.

The **EC-Na-metal** (1) particle type was very similar to cluster (3) from Turbofan 2. Also, contribution by this cluster, 23%, is comparable. The **metal-S-EC** (2) particle type comprises 18% of the particles. This cluster shows similar peaks to cluster (1), with less pronounced EC and more intense sulfate peaks. Moreover, it has more pronounced peaks from vanadium (m/z +51) and molybdenum (m/z +92 − +100). The **EC-S-metal** particle type (3) looked like cluster 1 from Turbofan 2. Both the clusters comprised the same number fraction of particles (44%). The **metal-N** particle type (4) made up of 12% of the total particles and was similar to cluster (2) for the Turbofan 2 with a distinct presence of barium. The **metal** particle type (5) comprised ~3% of the particles. As shown, a combination of metal compounds was detected in the positive spectrum, though the negative spectrum has major peaks that cannot be unambiguously assigned. The peak at m/z −43 is assigned to

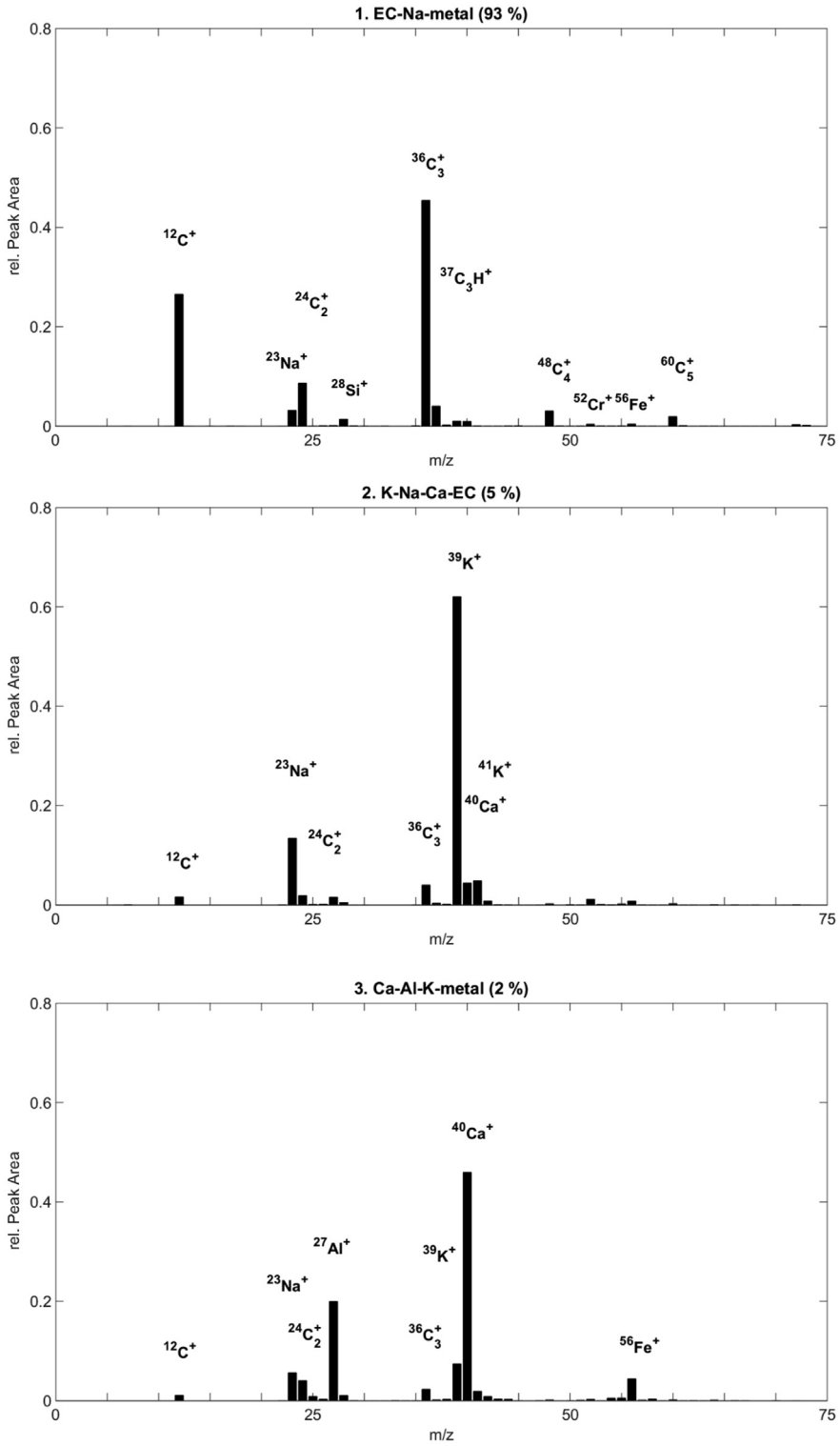

Fig. 4. The three major clusters (i.e. particle types) identified for particles emitted by Turbofan 1 during A-PRIDE 5.

C_2H_3O thus organic carbon (Spencer and Prather, 2006). The peak at m/z −42 was assigned to CNO, which could emerge due to the simultaneous occurrence of nitrogen and carbon in the particle (Mauney et al., 1984; Kolaitis et al., 1989). The peak at m/z −184 could not be assigned. This cluster does not have peaks associated with EC in either of the spectra. The sixth cluster (one spectra) had a dominant sulfate peak at m/z +97 and a peak at m/z −25 that could not be assigned.

3.2.5. Ambient background particles

ATOFMS measurements of ambient background particles were conducted in order to investigate if ambient aerosol particles could influence the engines measurements. The 325 background particles were sampled overnight from 6:00 p.m. to 9:00 a.m. without an

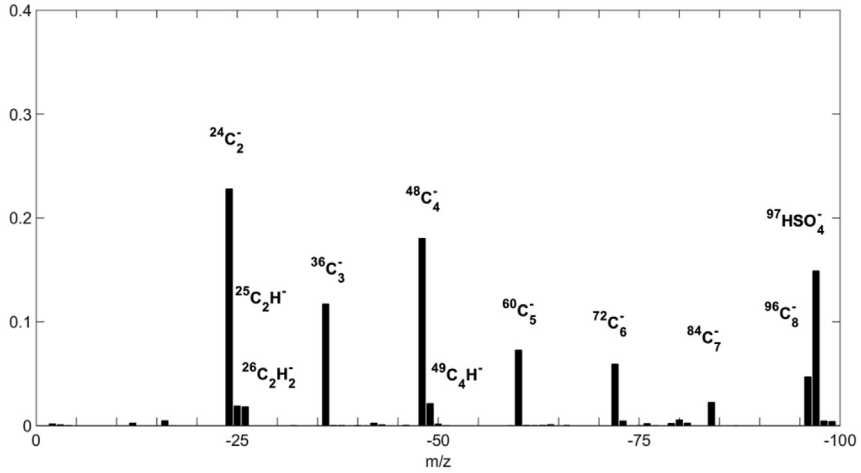

Fig. 5. Average negative spectrum from the spectra collected from the Turbofan 1 PM emissions.

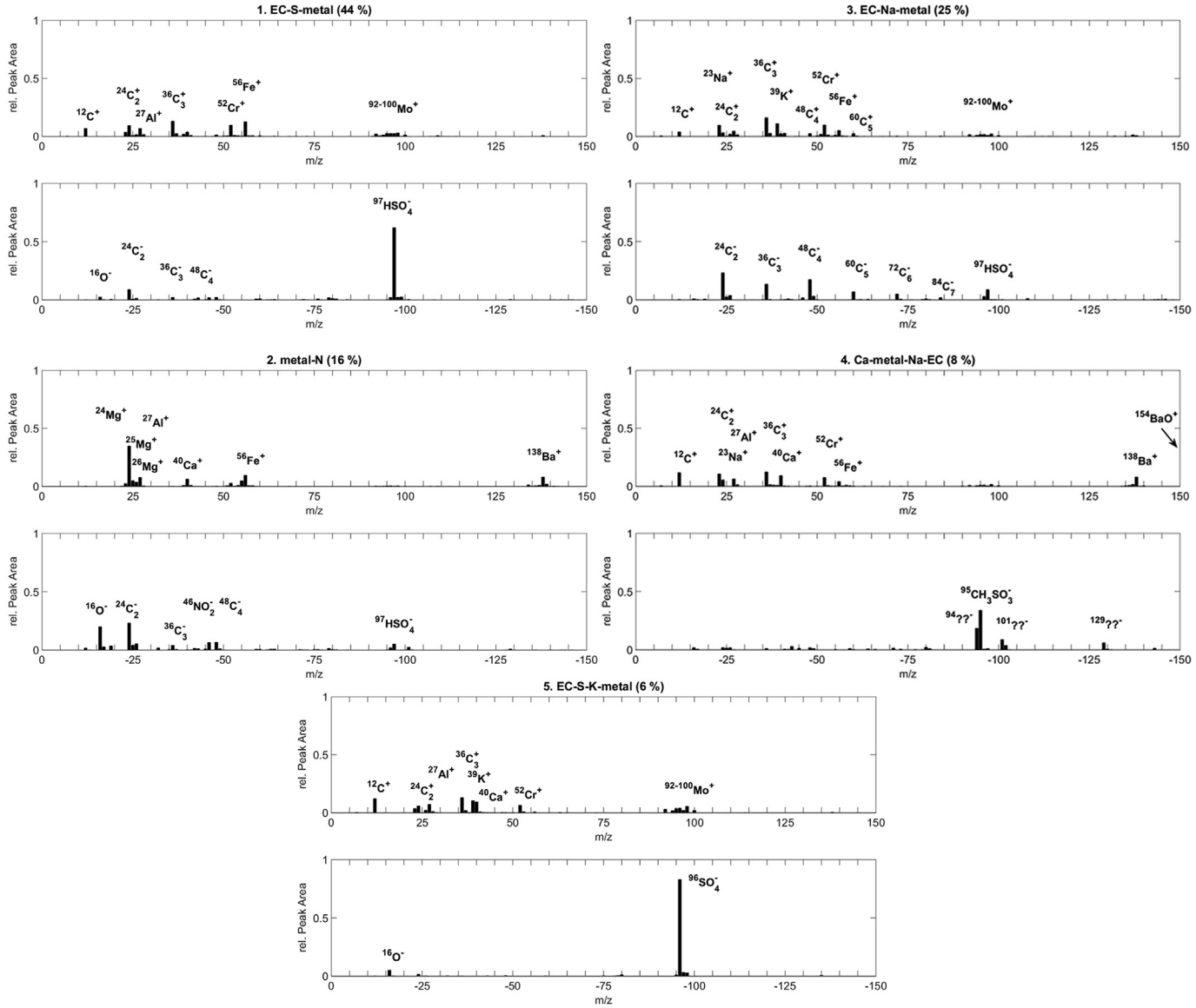

Fig. 6. Cluster analysis of the particle spectra measured from Turbofan 2 PM emissions, including both positive and negative spectra.

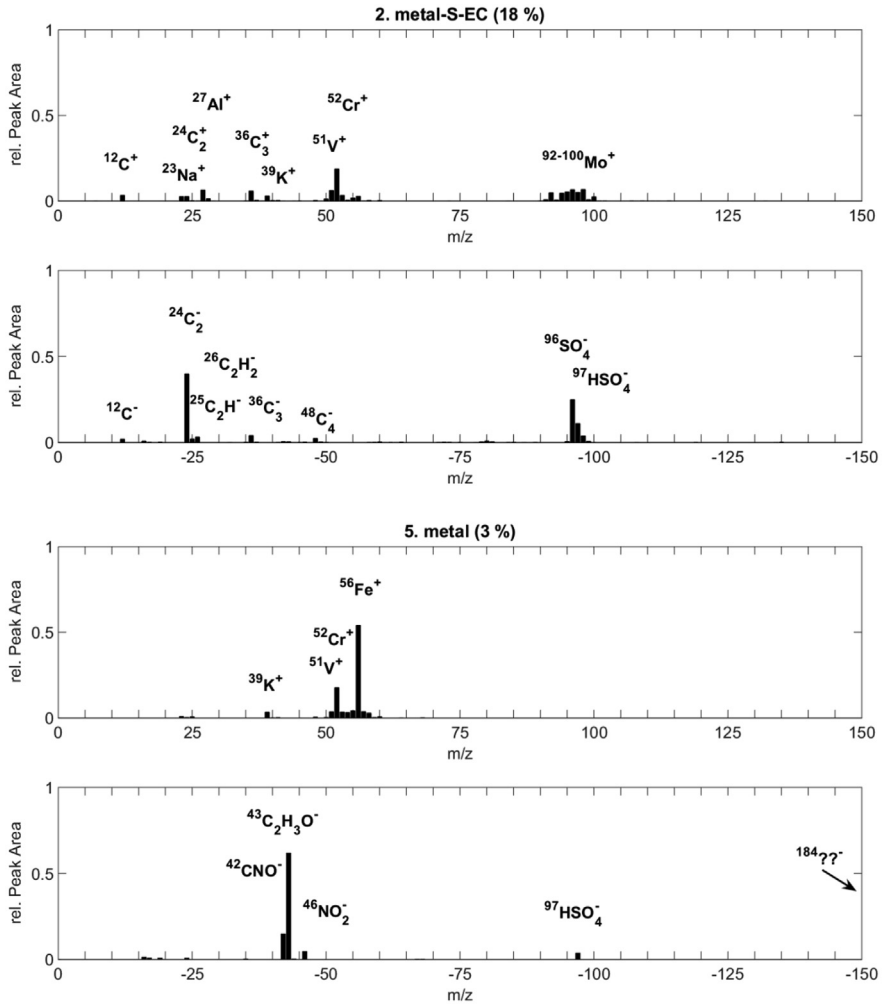

Fig. 7. Cluster analysis of the particle spectra measured from the Mixed-Flow Turbofan PM emissions.

engine running following the test run of the Mixed-Flow Turbofan which ended at 2:30 p.m. The sampled particles represent the aerosol particles that enter the test cell with the air that is consumed by the engine as it is running. During the overnight sampling, the airlocks of the test cell were left open to allow a passive exchange of the outside air with the test cell air. The sampling conditions did not fully reflect the situation during engine runs due to the flow of air through the test cell during engine runs caused by the operation of the engine.

In total, the analysis yielded seven clusters. The two main particle types are displayed in Fig. 8. The **K–N–Na** particle type (1) made up ~54% of the analyzed particles and has dominant potassium peaks at *m/z* +39 and + 41 and a smaller sodium peak. Calcium (*m/z* +40) is also present though this peak can be the result of the potassium signal at *m/z* +39 (especially if it is very intense) to which the ATOFMS is very sensitive (Healy et al., 2013) that sometimes causes a peak to be registered at *m/z* +40. The negative spectra are dominated by ion peaks from nitrate at *m/z* −46 and −62. A likely association with K, Na and N is dust (Jeong et al., 2011) probably from the road and the freeway nearby. The **S–Fe–K** particle type (2) comprises ~18% of the spectra. This cluster is dominated by a strong sulfate (*m/z* −97) signal and the presence of iron (*m/z* +56) and potassium ions (*m/z* +39). This cluster also has a weak EC signature in the positive mass spectra. Consequently, these particles could be aged remainders from aircraft exhaust emitted during previous engine tests or soot particles from sources nearby. The **K–N-EC** particle type (3) was made up of ~7% of the total spectra, and differed from the other clusters by its EC pattern up to C_9^- (*m/z* −108) mixed with potassium and nitrate. Additionally, it showed the metal compounds manganese (*m/z* +55) and iron (*m/z* +56). The **Fe–N** particle type (4) comprised ~7%. In contrast to the other clusters it displayed a prominent iron peak in the positive spectrum. The negative spectrum was dominated by a strong nitrate signal and a smaller sulfate peak. The **Ca–N–Na** particle type (5) comprised ~6% of the particles. Except for the presence of calcium instead of potassium, it had similar features than the K–N–Na particle type (1). The **EC-Ca-K-S** particle type (6) made up ~5% of the total particles. It depicted low intensities of carbonaceous peaks from EC mixed with potassium, calcium and sulfate, and in contrast to the other clusters, phosphate was detected, mainly at *m/z* −79 (PO_3) and to a smaller extent at *m/z* −63 (PO_2). These peaks are commonly associated with soil dust (Silva et al., 2000). The **K–C-N–N** particle type (7) only comprised ~2% of the total particles. This cluster had a strong potassium peak in the positive mass spectrum and peaks from organic nitrogen (*m/z* −26 (CN), −42 (CNO)) and nitrate (*m/z* −46, −62) in the negative spectra.

3.3. Elemental carbon to total carbon ratio

Elemental Carbon to Total Carbon ratios (EC/TC) were obtained

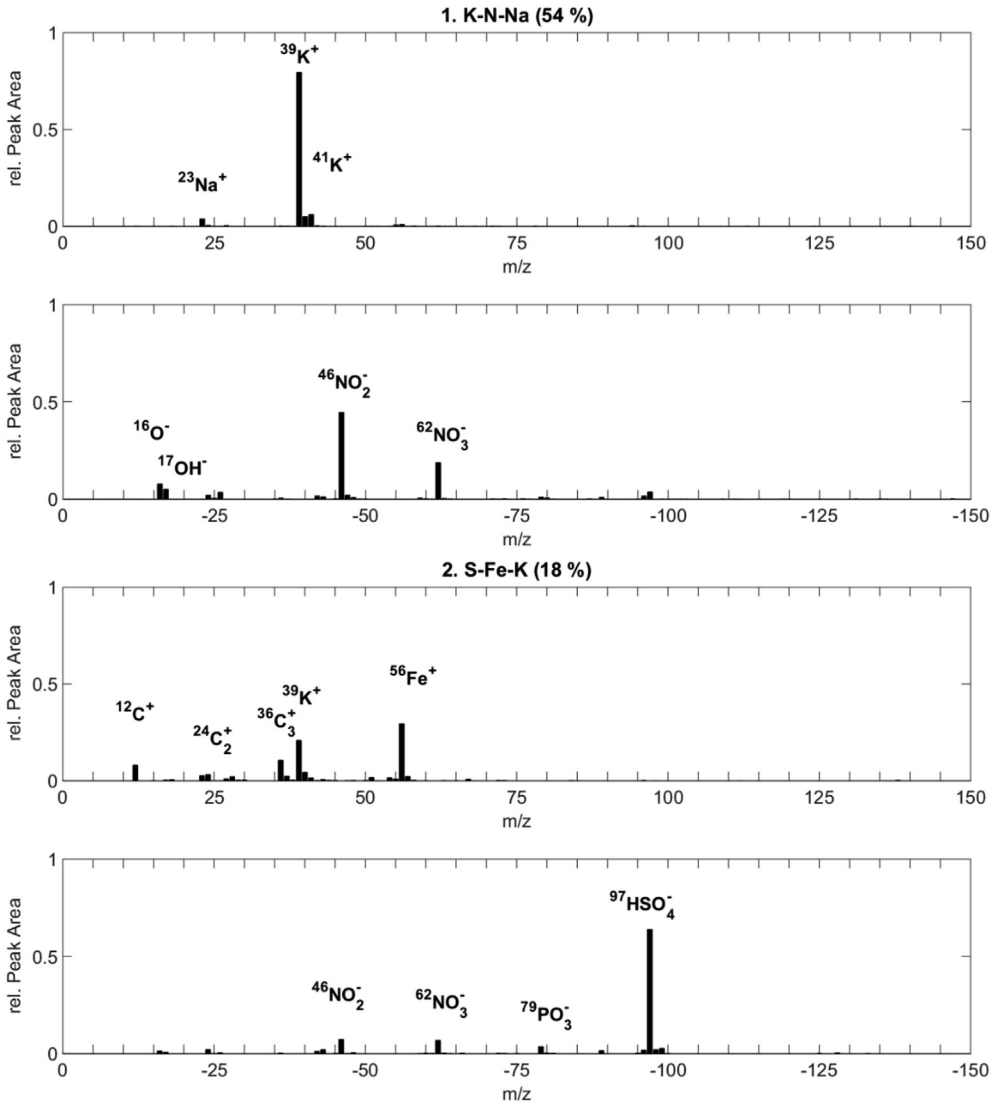

Fig. 8. Main clusters identified from the spectra collected during the ambient background measurements performed in the test cell without an engine running.

from positive ATOFMS spectra by adapting the method presented in Ferge et al. (2006). The thrust-dependent EC/TC ratios for the

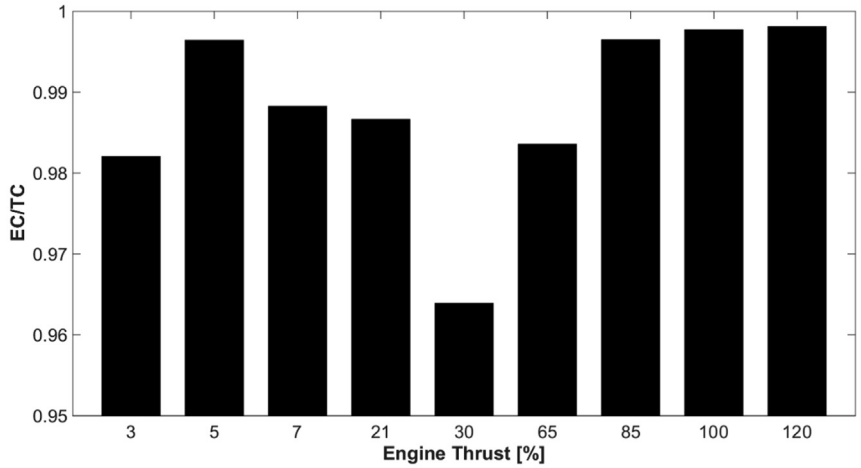

Fig. 9. Thrust dependent elemental carbon to total carbon values measured by the ATOFMS for Turbofan 1.

exhaust particles emitted by Turbofan 1 are displayed in Fig. 9. Depending on the applied thrust, the EC/TC ranged from 0.96 to almost 1 for the ATOFMS measured particles. The EC/TC ratios for the exhaust particles emitted by Turbofan 2 and the Mixed-Flow Turbofan were averaged over all measured thrust levels because the majority of the spectra were obtained at thrusts <30%. These were 0.89 and 0.83 respectively, considerably lower than for Turbofan 1. This implies that the relative contribution of OC to the TC in the emissions from Turbofan 1 is lower compared to the other two engines. We attribute these differences to different engine deteriorations. For comparison, Ferge et al. (2006) reported EC/TC values for soot samples of two different sizes of 0.90 (±0.05) and 0.89 (±0.03) from a diffusion flame generator using the setting for high organic loadings and 0.94 (±0.01) and 0.93 (±0.02) using the setting for low organic loadings.

The EC/TC ratios presented in this paper differ from literature results for aircraft engine exhaust particles. Agrawal et al. (2008) analyzed PM samples collected on filters and determined their EC and OC content using thermo-optical measurements. Also, Petzold and Schröder (1998) sampled jet engine exhaust on filters and determined the deposited mass of BC and OC using a thermal method. Both studies found a significantly higher contribution of OC to TC compared to the ATOFMS derived results, especially at low engine thrusts. The most likely reason for the high EC/TC values determined using the ATOFMS is that our analysis is solely based on the chemical composition of the largest particles emitted. Reaction rates leading to the oxidation of soot particles are usually described using the number of active sites on the particle surface (Neeft et al., 1997). Thus, it is reasonable to assume that the absolute OC content of a soot particle scales with particle surface area rather than with particle mass leading to a relatively smaller OC content in larger soot particles. This also agrees with the differences being larger at low engine thrusts when the emitted particles are generally smaller than at high thrusts (cf. Fig. 2). This difference was not observed for the particles analyzed by the ATOMFS. Moreover, the engine types investigated were not the same causing further differences of the EC/TC values presented herein.

For comparison, we calculated the number of particles associated with EC, classed as particles with peaks at m/z −36, −24, −12, +12, +24 and + 36. The number fractions of EC-containing particles emitted by Turbofan 1, Turbofan 2 and the Mixed-Flow Turbofan were 97.5%, 94.5% and 96.7%, respectively. Although the exhaust emitted by the Mixed-Flow Turbofan was mixed with bypass air (ambient air) the fraction of EC-containing particles was not smaller than for the exhaust particles emitted by Turbofan 2. This can be explained by the relative low particle concentration in the bypass air compared to the emitted soot particles in the core-flow. Also, the ambient air showed a significantly smaller fraction of EC-containing particles with most of these spectra showing weak EC signals. Thus, we concluded that the bypass air did not influence the fraction of EC-containing particles in the exhaust of the Mixed-Flow Turbofan. Moreover, this conclusion is supported by the finding that no particle type detected in the background air was identified for the particles emitted by the Mixed-Flow Turbofan (cf. 3.2.1).

For more detailed information on the carbon-containing particles, MS-Analyze was further used to classify the particles into 'EC' and 'ECOC' classes for Turbofan 1, depicted in Fig. 10 according to the applied thrust. The 'K noEC noOC' class consisted mainly of spectra from particles that showed a dominant potassium peak. The number fraction of the 'ECOC' class defined in this way has to be considered as the lower limit because of the possibility that some of the particles from the 'EC + K' class are actually 'ECOC'. The number fraction of the 'EC' class ranges from ~50% to ~90% where the highest values are found to occur in the high thrust range (85–120%). The 'K noEC noOC' class and 'unclassified' particles are the only ones not associated with EC, and were generally higher at thrust ≤30%. For the same engine type at thrust >30%, Brem et al. (2015) found that the influence of aromatic species from the Jet A-1 fuel on soot emissions decreases with increasing thrust. They attributed the observed maximum influence at 30% thrust to the less efficient combustion of aromatics, due to lower combustor temperatures and pressures. If this applies to organics in general, more organic material would remain unburnt at low thrust than at high thrust, which would explain the generally higher fraction of particles in the 'EC' class at higher thrusts.

3.4. Metals

3.4.1. Occurrence of metallic compounds

The following metallic compounds were detected to be internally mixed with the exhaust soot particles: molybdenum, calcium, sodium, iron, copper, barium, chromium, aluminium, silicon, magnesium, cobalt, manganese, vanadium, nickel, lead, titanium and zirconium. These metallic compounds were detected for all three engines investigated except for zirconium that was not found in particles from Turbofan 1. Also, indium, boron, selenium, arsenic, tin, wolfram, antimony and gadolinium were analyzed, but they were not detected except for antimony, boron and wolfram that were identified on only four or less particles each. In general, one or more metallic compounds were detected in a single particle, and the fraction of particles emitted by Turbofan 1 containing at least one, two, three and four metals was 36.3%, 19.9%, 10.5% and 3.2%, respectively.

The metals, number fractions and relative peak areas for the three engines and the ambient background measurements are listed in Table 1. The fractions for the Turbofan 1 engine are sorted according to the applied thrust to reveal variations between the different phases of an aircraft taxiing (low thrust), cruise (medium thrust) and take-off (high thrust). However, the actual cruise conditions are only partly represented by the medium thrust range as measured in the test cell because the inlet pressure and the fuel flow do not correspond to typical cruise values due to different ambient pressures and temperatures as well the missing forward speed. Moreover, the turbine case can shrink due to the low temperatures in high altitudes. Consequently, the results presented in the following for the medium thrust range should only be considered as indicative and not be used directly to describe the aircraft PM emissions during cruising conditions of an actual flight. The relative peak area value given in parenthesis is normalized for each metallic compound so that the largest peak area measured corresponds to 1 for that metal. The data for Turbofan 2 and the Mixed-Flow Turbofan were averaged over all measured thrusts because not enough particles were sampled for a thrust-dependent analysis. However, ~80% of these particles were sampled at thrusts <30% corresponding largely to the low thrust range.

For Turbofan 1 the fraction of particles containing molybdenum is largest at the high thrust range. Also within this range, the fraction was found to increase with increasing thrust. For calcium, sodium, iron, copper and barium the corresponding fractions of particles containing the metal are largest at low thrust and decrease with increasing thrust. A reason for this behavior could be the increasing total particle concentration with increasing thrust. If the total amount of these metallic compounds did not increase with increasing thrust, then relatively fewer particles are affected by them. For chromium, aluminium, silicon, magnesium, cobalt, vanadium, nickel, lead and titanium the corresponding fractions of particles containing the metal are largest at medium thrust. In contrary to the other compounds the peak area values from calcium and barium are not largest at that thrust range where the fraction of

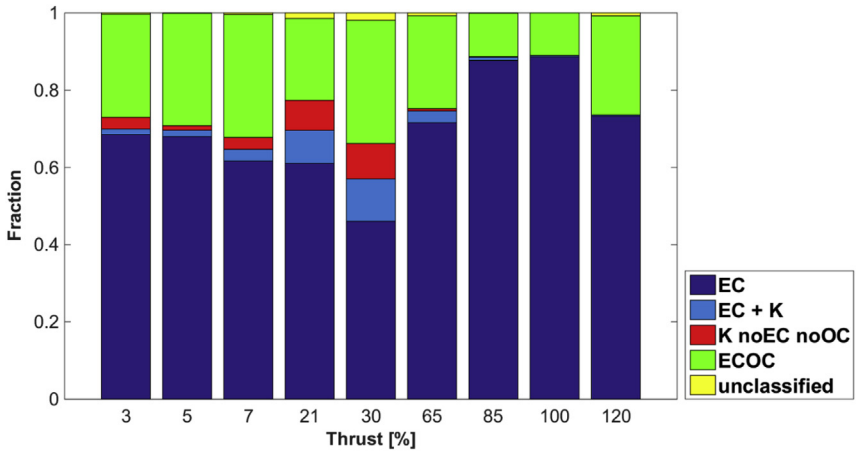

Fig. 10. Thrust dependent fraction of the particles from Turbofan 1 classified into 'EC' and 'ECOC'. The 'EC + K' and the 'K noEC noOC' classes were needed to define the 'ECOC' class.

Table 1
Number fraction in percent of spectra from particles emitted by the Turbofan 1, Mixed-Flow Turbofan and Turbofan 2 engines and from ambient background showing peaks indicating the presence of the corresponding metal compound. For Turbofan 1 the values are pooled into low (3–7%, idle/taxi), medium (20–65%, cruise) and high (85–120%, take-off) thrust range, and the value in parenthesis is the average peak area normalized to the largest value for each metal.

Element	Turbofan 1			Mixed-flow turbofan	Turbofan 2	Background
	Low thrust	Medium thrust	High thrust			
Molybdenum	5.3 (0.52)	5.9 (0.73)	9.6 (1.00)	55.9	36.7	1.9
Calcium	32.4 (0.61)	16.2 (1.00)	1.8 (0.04)	22.3	39.1	23.1
Sodium	29.1 (1.00)	22.6 (0.41)	4.3 (0.06)	50.2	51.1	34.5
Iron	22.5 (1.00)	8.4 (0.49)	0.7 (0.06)	33.0	35.5	11.1
Copper	2.9 (1.00)	0.4 (0.50)	0.0 (–)	2.6	6.7	2.5
Barium	0.5 (0.16)	0.3 (1.00)	0.1 (0.08)	3.7	16.5	2.2
Chromium	2.7 (0.10)	17.2 (1.00)	3.6 (0.18)	72.3	52.0	5.2
Aluminium	3.1 (0.21)	8.4 (1.00)	1.0 (0.03)	8.3	13.5	15.1
Silicon	0.4 (0.36)	2.1 (1.00)	0.1 (0.15)	0.2	0.9	4.3
Magnesium	0.6 (0.46)	1.7 (1.00)	0.3 (0.04)	16.6	20.8	3.1
Cobalt	0.5 (0.83)	1.4 (1.00)	0.4 (0.93)	1.7	2.8	1.5
Manganese	0.3 (0.84)	0.9 (1.00)	0.1 (0.02)	17.5	17.4	8.9
Vanadium	0.4 (0.89)	0.7 (1.00)	0.1 (0.04)	9.4	9.2	3.4
Nickel	0.4 (0.12)	0.6 (1.00)	0.1 (0.04)	10.7	19.3	8.3
Lead	0.1 (0.36)	0.4 (1.00)	0.0 (–)	1.3	0.9	2.5
Titanium	0.0 (–)	0.2 (1.00)	0.0 (–)	0.0	0.9	0.0
Zirconium	0.0 (–)	0.0 (–)	0.0 (–)	0.9	0.6	0.3

calcium- and barium-containing particles are largest. This indicates that the amount of calcium and barium present on each particle is largest at medium thrust despite the smaller number fractions.

The fractions of metal-containing particles were generally higher for Turbofan 2 and the Mixed-Flow Turbofan than for the Turbofan 1 with the largest differences found for molybdenum, barium, chromium, aluminium, manganese, magnesium, vanadium, nickel and lead. As discussed in the next section, kerosene, lubrication oil, grease and engine wear are potential sources of these metals. One reason for the larger fractions is the possible difference in oil and grease consumption. Turbofan 2 and the Mixed Flow Turbofan generally have a higher oil consumption than Turbofan 1. Another reason for the differences in the measured metal-containing fractions are variations thereof over time for the same engine. Alloys sometimes consist of heterogeneously distributed compounds. Thus, if wear takes place and an engine alloy frets, its individual compounds are unevenly released. Also, it is known that an engine can exhibit an increased abrasion of wearing components during the beginning of the first operation after it was overhauled. From the work scope of the investigated engines we do not expect this to be the case, however, increased abrasion can still not be entirely excluded.

The presented fractions of particles that contain metallic compounds are lowest for the ambient background particles except for silicon, lead and aluminium of which the latter shows similar values as Turbofan 1. It is likely that the ambient background measurements were influenced to some extent by the engine test run conducted beforehand on the Mixed-Flow Turbofan.

3.4.2. Potential sources of metals

ICP-MS was conducted to investigate potential sources of the metallic compounds identified in the exhaust particles of aircraft engines. It was applied as quantitative element screening on a) kerosene (Jet A-1 Fuel), b) engine lubrication oil (Mobile Jet II) and c) debris from engine wearing components.

Kerosene and oil samples were taken from the batch actually consumed by the aircraft engine during the A-PRIDE 5 campaign. As a reference for material from engine wearing components, a sample of debris collected on the blades of the High Pressure Turbine (HPT) of another Turbofan 1 engine type was used. The HPT is located downstream of the combustor where the collected debris was carried and accumulated by combustor air. The influence of oil on the emissions is thought to be less important compared to kerosene because of the much smaller amounts consumed. The ratio of

kerosene to oil consumption is estimated to be ~5000 (±1500):1 for the tested engines at medium thrust. Another potential source of the identified metal compounds in the exhaust not analyzed herein is grease mainly applied to rotating engine parts.

The detection of silicon in kerosene and oil samples using ICP-MS was not possible because of the analytical procedure applied. The concentrations in milligram per kilogram [mg/kg] of the most abundant metallic elements in Jet A-1 Fuel and Mobile Jet II Oil are shown in Table 2. 'Others' comprise compounds with >0.1 mg/kg each, including barium, manganese, arsenic, tin, nickel and molybdenum detected in both fuel and oil, whereas indium and boron were solely detected in fuel, and selenium solely in oil. Besides the metallic elements, sulphur and phosphorus were also detected in both samples.

The elements that were detected in the solid HPT debris using ICP-MS are shown in Table 3 in percentage of mass [wt%]. It only lists the elements detected in the exhaust particles as well, covering 98.2% of the mass of the HPT debris sample. The debris was stored in 95% ethanol and 5% isopropyl alcohol after sampling and a potential contamination from the solvent cannot be excluded. The suspension was homogenized and dried directly before the analysis.

The ICP-MS results of the HPT debris was used to reveal compounds that are probably from engine wear. Although the identified compounds were part of the combustion air, the actual composition of the HPT debris as it was collected has not contributed to the combustion process like kerosene and oil. From empirical values the HPT debris was accumulated in the engine over an estimated engine operation time of about 20,000 h to 30,000 h. During this time, huge amounts of air passed through the HPT, allowing the accumulation of compounds not only from engine processes such as wear or kerosene and oil residues but probably also from ambient aerosol collected during flight. We assume silicon, calcium and sodium from ambient air to cause the large weight fractions in the HPT debris.

A potential source of aircraft engine wear are the so-called honeycomb structures that are built into in the compressor region of the engine downstream the combustor. The honeycomb structures are a wearing part made out of 'Hastelloy X'. The chemical composition and the corresponding weight fractions in percentages (in parenthesis) according to the specification sheet (Haynes, 1997) is: Ni (47), Cr (22), Fe (18), Mo (9), Co (1.5), W (0.6), Mn (≤1), Si (≤1), B (≤0.008). It was suggested that wear from 'Hastelloy X' contribute to debris collected in the HPT. However, the relative large amounts of molybdenum in 'Hastelloy X' and the large fractions of exhaust particles containing molybdenum are not reflected in the small mass fraction of molybdenum found in HPT debris. Thus, the amount of 'Hastelloy X' in HPT debris is probably rather small. Nevertheless, this does not exclude the possibility of wear from 'Hastelloy X' to contribute to the metals identified in the exhaust particles. Below, we discuss potential sources for each individual metal compound identified in the emitted engine particles based on the ICP-MS analyses.

Table 2
Concentrations in milligram per kilogram [mg/kg] of the most abundant metallic elements in the sampled Jet A-1 fuel and Mobile Jet II oil detected using ICP-MS.

Element	Jet A-1 fuel	Mobile Jet II oil
Calcium	113.15	30.82
Vanadium	3.59	1.82
Aluminium	3.08	4.35
Lead	1.98	>0.1
Iron	1.69	1.77
Magnesium	1.46	2.25
Titanium	1.45	6.01
Sodium	1.05	1.28
Copper	0.96	(–)
Antimony	>0.1	1.15
Chromium	(–)	1.09
Others	4.91	5.3

Table 3
Mass fractions in percentage of mass [wt%] and 95% confidence intervals (CI) of elements in solid residue from the HPT debris obtained using ICP-MS.

Element	Mass fraction, CI (95%)
Silicon	60.1, [59.6, 60.6]
Calcium	12.2, [11.4, 13.0]
Sodium	5.03, [4.88, 5.18]
Iron	5.00, [4.65, 5.35]
Aluminium	4.90, [4.60, 5.20]
Magnesium	4.00, [3.90, 4.10]
Nickel	3.43, [3.39, 3.47]
Chromium	0.90 [0.86, 0.94]
Titanium	0.63 [0.61, 0.65]
Manganese	0.39 [0.39, 0.40]
Lead	0.39 [0.37, 0.41]
Copper	0.48 [0.45, 0.51]
Cobalt	0.32 [0.32, 0.33]
Barium	0.20 [0.17, 0.23]
Molybdenum	0.18 [0.17, 0.19]
Vanadium	0.051 [0.049, 0.053]
Zirconium	0.017 [0.012, 0.022]

3.4.2.1. Exclusively engine wear. **Zirconium** was detected in small amounts in HPT debris but not in kerosene or oil. It is known to be used as thermal barrier coating in aircraft engine parts (Miller, 1997). **Cobalt** was detected in small amounts in HPT debris and it is used in 'Hastelloy X' but not in kerosene or oil.

3.4.2.2. Mainly engine wear. **Iron** was detected in substantial amounts in HPT debris and in 'Hastelloy X'. It was also found in kerosene and in oil. Compared to other metallic compounds such as vanadium, lead, magnesium and titanium the number fraction of iron-containing particles was relatively high whereas the amounts detected in kerosene and oil were similar. Thus, we assume this difference in the fraction to be caused by the higher iron content in HPT debris and in 'Hastelloy X'. **Copper** was detected in kerosene and it is used in 'Hastelloy X'. Copper was not detected in oil. It was detected in the exhaust particles mainly in combination with iron indicating engine wear as a major source. **Chromium** was detected in HPT debris and 'Hastelloy X' contains a weight fraction of 22%. Chromium is widely used in engine parts e.g. aircraft turbine blades and alloys. It was detected in oil but not in kerosene. **Nickel** is the most abundant constituent of 'Hastelloy X' and it shows a substantial weight fraction of 3.4% in HPT debris. Only very low concentrations of nickel were detected in kerosene and in oil. **Molybdenum** is a main constituent of 'Hastelloy X'. However, in aerospace, molybdenum disulfide is widely used in grease for lubrication applications where metal to metal contact exists. It can be converted directly to molybdenum metal when heated (Epshteyn and Risdon, 2010). The highest number fraction of molybdenum-containing particles was measured at maximum thrust when grease consumption and engine wear are likely to be highest. Only small quantities were detected in kerosene and oil. We therefore assume molybdenum to originate mainly from engine wear and grease.

3.4.2.3. Mainly kerosene. **Barium** was detected in kerosene and in oil. It is not supposed to be present in any engine parts. As a side note, because of its capability to reduce soot emissions in

combustion processes (Howard and Kausch, 1980) by acting as a nucleation core for soot it was earlier used as an antismoke additive in kerosene to reduce the smoke number. **Vanadium** was detected in kerosene and in oil. Engine wear as a source of vanadium is not significant due to the very small amount detected in HPT debris. **Lead** was mainly detected in kerosene and only small amounts were detected in oil and in HPT debris. Lead is not used in any engine parts. **Titanium** was detected in kerosene and in oil. Small amount were also detected in HPT debris may be from alloys used in the compressor of aircraft engine upstream of the combustor. **Calcium** and **sodium** were both detected in kerosene and in oil. Especially calcium was detected in relatively large concentrations. Both kerosene and oil probably contribute to their existence in the exhaust particles. Calcium and sodium originating from engine wear can be excluded because they are not used in any engine part. However, ambient aerosol as an additional source is also possible because of the large fraction of ambient background particles containing calcium and/or sodium and the possibility that these compounds are redistributed onto the exhaust particles via gas phase processes.

3.4.2.4. No main source identified. **Aluminium** was detected in kerosene, in oil and in HPT debris. Also, it is used in many engine parts. **Silicon** could not be identified with the ICP-MS method applied to the kerosene and oil samples. Small amounts of silicon are used in many materials used in aircraft engines. **Magnesium** was detected in oil, kerosene and HPT debris which are all potential sources. **Manganese** was detected in small amounts in oil, kerosene and HPT debris. Similar to silicone, it is commonly present in engine parts.

4. Summary and conclusions

We investigated the chemical composition of single particles emitted from three different in-production aircraft turbofan engines using an ATOFMS. Particle types were identified using a data mining software enabling the analysis of atmospheric mass spectra. The bulk EC/TC ratios were determined. Furthermore, we determined the fractions of particles that contained metallic compounds. In order to identify sources of the metallic compounds ICP-MS was performed on samples from Jet A-1 fuel, Mobile Jet II and debris from engine wearing components. The particles that were analyzed by the ATOFMS represented a subset of the non-volatile emissions composing only the largest particles due to instrumental restrictions.

Depending on engine type, 94.5%–97.5% of the particles contained EC. All three engine types showed common similar particle types regarding their chemical composition and corresponding number fractions. These were the EC-Na metal, EC-S-metal and Metal-N particle types. The thrust-dependent EC/TC ratio of the emissions from Turbofan 1 ranged from 0.96 up to more than 0.99 depending on the applied thrust. The EC/TC ratio of the emissions from Turbofan 2 and the Mixed-Flow Turbofan were 0.89 and 0.83, respectively. These results were not influenced by whether the engine was a core flow engine or a mixed flow engine. The EC/TC values are considerably higher than reported by Petzold and Schröder (1998) and Agrawal et al. (2008) for PM aircraft exhaust emitted by other engine types, especially at low thrust. This difference is likely caused by the ATOFMS analyzing the fraction of the largest particles emitted in which the relative OC content is assumed to be smaller.

Particles containing metallic compounds were all internally mixed with the soot. The following compounds were detected in particles from all engines: Cr, Fe, Mo, Na, Ca, Al, V, Ba, Co, Cu, Ni, Pb, Mg, Mn, Si and Ti. Zr was only detected in the Turbofan 2 and Mixed-Flow Turbofan exhaust. The fraction of metal-containing particles was lower for the Turbofan 1 than for the Turbofan 2 and the Mixed-Flow Turbofan. To identify sources of the metallic compounds ICP-MS analyses were carried out. Traces of all compounds were detected in kerosene and/or in oil except for Co and Zr. We conclude that cobalt and zirconium can possibly be used as tracers for aircraft exhaust because they solely originate from engine wear. This accounts especially for cobalt because it was detected in the emission from all of three engines investigated. However, this would require further research because other combustion sources of cobalt- and zirconium-containing soot particles cannot be completely excluded. Nevertheless, the combined usage of cobalt and zirconium is rather limited. To use the other detected compounds as tracers is not possible because diesel and petroleum are produced from crude oil just like kerosene. Thus, the metallic compounds detected in kerosene can be expected to be found in other fuels and emissions, too.

In general, an unambiguous source apportionment of the metal compounds detected in the engine exhaust particles is difficult because of multiple reasons. Most importantly, many metals are detected at least in small amounts in multiple potential sources. Also, there is the possibility that the element composition of fuel and lubrication oil varies due to contamination in storage and distribution facilities (Fordyce and Sheibley, 1975). Further, it is difficult to quantitatively relate the sources to the compounds detected in the particles. On the one hand, the relative extents of the contribution from the individual sources are not exactly known. This is partly because aircraft engines are a complex system where exploration of chemo physical processes of trace elements within the engine is difficult because no direct observations are possible. On the other hand, the ATOFMS data is non-quantitative and represent only the largest exhaust particles. Moreover, engine wear and oil and grease consumption are not constant over the lifetime of an aircraft engine.

The implications of our results are of importance due to the potential of metal-containing particles to act as INP and consequently impact cirrus cloud properties and thus global climate (Cziczo et al., 2013). As a minimum value among the three engines, 36% of the particles emitted by Turbofan 1 contained at least one metallic compound. These finding suggest that aircraft engine emissions are a considerable source of potential INP in the atmosphere. The fractions of metal-containing particles did not show a size-dependence in our investigated size-range in agreement with Demirdjian et al. (2007) who also did not observe appreciable differences in the chemical composition between small and large soot particles sampled directly behind an aircraft gas turbine engine. The majority of the actual aircraft emissions take place in the upper troposphere where the aircraft operate mainly at cruise conditions that can be mimicked to a certain degree with the medium thrust range measured in the engine test cell. Our thrust-dependent analysis revealed that for most of the metallic compounds, the measured averaged relative peak areas were found to be largest at medium thrust. This indicates that also their contents in the soot particles are largest at medium thrust. If the presence of a metallic compound is responsible for the INP activity of a soot particle, a larger content probably enhances its effectiveness to act as INP. At medium thrust range, measurements of the emissions showed high particle concentrations of $>10^6$ cm^{-3} (Abegglen et al., 2015) for Turbofan 1. In the upper troposphere the concentration of INP is typically on the order of <0.01 cm^{-3} (DeMott et al., 2003) where additional INP would contribute substantially to the total number, potentially resulting in significant cirrus modifications (Hendricks et al., 2005, 2011). Therefore, to understand the connection between metal-containing particles from aircraft exhaust and ice nucleation, we recommend investigation of the ice-

nucleating properties of non-volatile aircraft emissions. In addition, our findings provide information with regard to human health effects from aircraft PM emissions potentially caused by trace metals contained in the particles.

Acknowledgements

This study was made possible with funding from the Swiss Federal Office of Civil Aviation through the project "Particulate Matter and Gas Phase Emission Measurement of Aircraft Engine Exhaust" (Grant No. SFLV 2012-004). The A-PRIDE 5 engine lease was partially funded by the European Aviation Safety Agency and the US Federal Aviation Administration and Transport Canada under Grant No. 09-C-NE-MST Amendments 011 and 014. We are grateful for the help and technical assistance provided by SR Technics, especially Frithjof Siegerist and the test cell crew. Also, we thank Adrian Wichser from Empa and Bodo Hattendorf from ETHZ and appreciate their contribution by performing the ICP-MS analyses of our fuel/oil samples and our HPT debris, respectively. Lastly, we thank Fabian Mahrt for his effort to support the maintenance of the ATOFMS.

References

Abegglen, M., Durdina, L., Brem, B.T., Wang, J., Rindlisbacher, T., Corbin, J.C., Lohmann, U., Sierau, B., 2015. Effective density and mass–mobility exponents of particulate matter in aircraft turbine exhaust: dependence on engine thrust and particle size. J. Aerosol Sci. 88, 135–147. http://dx.doi.org/10.1016/j.jaerosci.2015.06.003.

Agrawal, H., Sawant, A.A., Jansen, K., Wayne Miller, J., Cocker Iii, D.R., 2008. Characterization of chemical and particulate emissions from aircraft engines. Atmos. Environ. 42 (18), 4380–4392. http://dx.doi.org/10.1016/j.atmosenv.2008.01.069.

Birch, M.E., 2002. Occupational monitoring of particulate diesel exhaust by NIOSH method 5040. Appl. Occup. Environ. Hyg. 17 (6), 400–405. http://dx.doi.org/10.1080/10473220290035390.

Boies, A.M., Stettler, M.E.J., Swanson, J.J., Johnson, T.J., Olfert, J.S., Johnson, M., Eggersdorfer, M.L., Rindlisbacher, T., Wang, J., Thomson, K., Smallwood, G., Sevcenco, Y., Walters, D., Williams, P.I., Corbin, J., Mensah, A.A., Symonds, J., Dastanpour, R., Rogak, S.N., 2015. Particle Emission characteristics of a gas turbine with a double annular combustor. Aerosol Sci. Technol. 49 (9), 842–855. http://dx.doi.org/10.1080/02786826.2015.1078452.

Braun, A., Huggins, F.E., Seifert, S., Ilavsky, J., Shah, N., Kelly, K.E., Sarofim, A., Huffman, G.P., 2004. Size-range analysis of diesel soot with ultra-small angle X-ray scattering. Combust. Flame 137 (1–2), 63–72. http://dx.doi.org/10.1016/j.combustflame.2004.01.003.

Brem, B., Durdina, L., Siegerist, F., Beyerle, P., Bruderer, K., Rindlisbacher, T., Rocci Denis, S., Andac, M.G., Zelina, J., Penanhoat, O., Wang, J., 2015. Effects of fuel aromatic content on non-volatile particulate emissions of an in-production aircraft gas turbine. Environ. Sci. Technol. http://dx.doi.org/10.1021/acs.est.5b04167.

Burkhardt, U., Kärcher, B., 2011. Global radiative forcing from contrail cirrus. Nat. Clim. Change 1, 54–58. http://dx.doi.org/10.1038/nclimate1068.

Corporan, E., Quick, A., DeWitt, M.J., 2008. Characterization of particulate matter and gaseous emissions of a C-130H aircraft. J. Air Waste Manag. Assoc. 58 (4), 474–483.

Cozic, J., Mertes, S., Verheggen, B., Cziczo, D.J., Gallavardin, S.J., Walter, S., Baltensperger, U., Weingartner, E., 2008. Black carbon enrichment in atmospheric ice particle residuals observed in lower tropospheric mixed phase clouds. J. Geophys. Res. Atmos. 113 (D15) http://dx.doi.org/10.1029/2007JD009266.

Cziczo, D.J., Froyd, K.D., Hoose, C., Jensen, E.J., Diao, M., Zondlo, M.A., Smith, J.B., Twohy, C.H., Murphy, D.M., 2013. Clarifying the dominant sources and mechanisms of cirrus cloud formation. Science 340 (6138), 1320–1324. http://dx.doi.org/10.1126/science.1234145.

Cziczo, D.J., Stetzer, O., Worringen, A., Ebert, M., Weinbruch, S., Kamphus, M., Gallavardin, S.J., Curtius, J., Borrmann, S., Froyd, K.D., Mertes, S., Mohler, O., Lohmann, U., 2009. Inadvertent climate modification due to anthropogenic lead. Nat. Geosci. 2 (5), 333–336. http://www.nature.com/ngeo/journal/v2/n5/suppinfo/ngeo499_S1.html.

DeCarlo, P.F., Slowik, J.G., Worsnop, D.R., Davidovits, P., Jimenez, J.L., 2004. Particle morphology and density characterization by combined mobility and aerodynamic diameter measurements. Part 1: Theory. Aerosol Sci. Technol. 38, 1185–1205. http://dx.doi.org/10.1080/027868290903907.

Demirdjian, B., Ferry, D., Suzanne, J., Popovicheva, O.B., Persiantseva, N.M., Shonija, N.K., 2007. Heterogeneities in the microstructure and composition of aircraft engine combustor soot: impact on the water uptake. J. Atmos. Chem. 56 (1), 83–103. http://dx.doi.org/10.1007/s10874-006-9043-9.

DeMott, P.J., 1990. An exploratory study of ice nucleation by soot aerosols. J. Appl. Meteorol. 29 (10), 1072–1079. http://dx.doi.org/10.1175/1520-0450(1990)029<1072:AESOIN>2.0.CO;2.

DeMott, P.J., Cziczo, D.J., Prenni, A.J., Murphy, D.M., Kreidenweis, S.M., Thomson, D.S., Borys, R., Rogers, D.C., 2003. Measurements of the concentration and composition of nuclei for cirrus formation. Proc. Natl. Acad. Sci. 100 (25), 14655–14660. http://dx.doi.org/10.1073/pnas.2532677100.

Diehl, K., Mitra, S.K., 1998. A laboratory study of the effects of a kerosene-burner exhaust on ice nucleation and the evaporation rate of ice crystals. Atmos. Environ. 32 (18), 3145–3151. http://dx.doi.org/10.1016/S1352-2310(97)00467-6.

Duda, D.P., Minnis, P., Khlopenkov, K., Chee, T.L., Boeke, R., 2013. Estimation of 2006 northern hemisphere contrail coverage using MODIS data. Geophys. Res. Lett. 40 (3), 612–617. http://dx.doi.org/10.1002/grl.50097.

Durdina, L., Brem, B.T., Abegglen, M., Lobo, P., Rindlisbacher, T., Thomson, K.A., Smallwood, G.J., Hagen, D.E., Sierau, B., Wang, J., 2014. Determination of PM mass emissions from an aircraft turbine engine using particle effective density. Atmos. Environ. 99, 500–507. http://dx.doi.org/10.1016/j.atmosenv.2014.10.018.

Epshteyn, Y., Risdon, T.J., 2010. Molybdenum disulfide in lubricant applications – a review. In: The 12th Lubricating Grease Conference (NLGI-India Chapter), pp. 1–12 (Goa, India).

Ferge, T., Karg, E., Schröppel, A., Coffee, K.R., Tobias, H.J., Frank, M., Gard, E.E., Zimmermann, R., 2006. Fast determination of the relative elemental and organic carbon content of aerosol samples by on-line single-particle aerosol time-of-flight mass spectrometry. Environ. Sci. Technol. 40, 3327–3335. http://dx.doi.org/10.1021/es050799k.

Fordyce, J.S., Sheibley, D.W., 1975. Estimate of contribution of jet aircraft operations to trace element concentration at or near airports. J. Air Pollut. Control Assoc. 25 (7), 721–724. http://dx.doi.org/10.1080/00022470.1975.10470131.

Gard, E., Mayer, J.E., Morrical, B.D., Dienes, T., Fergenson, D.P., Prather, K.A., 1997. Real-time analysis of individual atmospheric aerosol particles: design and performance of a portable ATOFMS. Anal. Chem. 69 (20), 4083–4091. http://dx.doi.org/10.1021/ac970540n.

Giorio, C., Tapparo, A., Dall'Osto, M., Harrison, R.M., Beddows, D.C.S., Di Marco, C., Nemitz, E., 2012. Comparison of three techniques for analysis of data from an aerosol time-of-flight mass spectrometer. Atmos. Environ. 61, 316–326. http://dx.doi.org/10.1016/j.atmosenv.2012.07.054.

Gross, D.S., Atlas, R., Rzeszotarski, J., Turetsky, E., Christensen, J., Benzaid, S., Olson, J., Smith, T., Steinberg, L., Sulman, J., Ritz, A., Anderson, B., Nelson, C., Musicant, D.R., Chen, L., Snyder, D.C., Schauer, J.J., 2010. Environmental chemistry through intelligent atmospheric data analysis. Environ. Model. Softw. 25 (6), 760–769. http://dx.doi.org/10.1016/j.envsoft.2009.12.001.

Gross, D.S., Gälli, M.E., Silva, P.J., Prather, K.A., 2000. Relative sensitivity factors for alkali metal and ammonium cations in single-particle aerosol time-of-flight mass spectra. Anal. Chem. 72 (2), 416–422. http://dx.doi.org/10.1021/ac990434g.

Gross, J.H., 2011. Mass Spectrometry: a Textbook, second ed. Springer, Berlin Heidelberg.

Han, C., Liu, Y., Ma, J., He, H., 2012. Key role of organic carbon in the sunlight-enhanced atmospheric aging of soot by O(2). Proc. Natl. Acad. Sci. U. S. A. 109 (52), 21250–21255. http://dx.doi.org/10.1073/pnas.1212690110.

Hatch, L.E., Pratt, K.A., Huffman, J.A., Jimenez, J.L., Prather, K.A., 2014. Impacts of aerosol aging on laser desorption/ionization in single-particle mass spectrometers. Aerosol Sci. Technol. 48 (10), 1050–1058. http://dx.doi.org/10.1080/02786826.2014.955907.

Haynes, I., 1997. Hastelloy® X Alloy [Brochure]. Author, Kokomo, IN.

Healy, R.M., Sciare, J., Poulain, L., Crippa, M., Wiedensohler, A., Prévôt, A.S.H., Baltensperger, U., SC-Estève, R., McGuire, M.L., Jeong, C.H., McGillicuddy, E., O'Connor, I.P., Sodeau, J.R., Evans, G.J., Wenger, J.C., 2013. Quantitative determination of carbonaceous particle mixing state in Paris using single-particle mass spectrometer and aerosol mass spectrometer measurements. Atmos. Chem. Phys. 13 (18), 9479–9496. http://dx.doi.org/10.5194/acp-13-9479-2013.

Hendricks, J., Kärcher, B., Lohmann, U., 2011. Effects of ice nuclei on cirrus clouds in a global climate model. J. Geophys. Res. Atmos. 116 (D18) http://dx.doi.org/10.1029/2010JD015302.

Hendricks, J., Kärcher, B., Lohmann, U., Ponater, M., 2005. Do aircraft black carbon emissions affect cirrus clouds on the global scale? Geophys. Res. Lett. 32 (12) http://dx.doi.org/10.1029/2005GL022740.

Herndon, S.C., Jayne, J.T., Lobo, P., Onasch, T.B., Fleming, G., Hagen, D.E., Whitefield, P.D., Miake-Lye, R.C., 2008. Commercial aircraft engine emissions characterization of in-use aircraft at Hartsfield-Jackson Atlanta international airport. Environ. Sci. Technol. 42, 1877–1883. http://dx.doi.org/10.1021/es072029+.

Howard, J.B., Kausch Jr., W.J., 1980. Soot control by fuel additives. Prog. Energy Combust. Sci. 6 (3), 263–276. http://dx.doi.org/10.1016/0360-1285(80)90018-0.

ICAO, 2008. Annex 16 to the Convention on International Civil Aviation: Environmental Protection, third, vol. II. Aircraft Engine Emissions.

ICAO, 2013. Environmental Report (Aviation and Climate Change).

IPCC, 1999. In: Penner, J.E., Lister, D.H., Griggs, D.J., Dokken, D.J., McFarland, M. (Eds.), Aviation and the Global Atmosphere. A Special Report of Intergovernmental Panel on Climate Change Working Groups I and III. Cambridge University Press, UK, Cambridge, UK and New York, NY, USA.

IPCC, 2007. In: Solomon, S., Qin, D., Manning, M., Chen, Z., Marquis, M., Averyt, K.B., Tignor, M., Miller, H.L. (Eds.), Climate Change 2007-The Physical Science Basis: Working Group I Contribution to the Fourth Assessment Report of the Intergovernmental Panel on Climate Change. Cambridge University Press, UK.

Janssen, N.A., Gerlofs-Nijland, M.E., Lanki, T., Salonen, R.O., Cassee, F., Hoek, G., Fischer, P., Brunekreef, B., Krzyzanowski, M., 2012. Health Effects of Black Carbon. World Health Organization, Copenhagen.

Jeong, C.H., McGuire, M.L., Godri, K.J., Slowik, J.G., Rehbein, P.J.G., Evans, G.J., 2011. Quantification of aerosol chemical composition using continuous single particle measurements. Atmos. Chem. Phys. 11 (14), 7027–7044. http://dx.doi.org/10.5194/acp-11-7027-2011.

Kärcher, B., Möhler, O., DeMott, P.J., Pechtl, S., Yu, F., 2007. Insights into the role of soot aerosols in cirrus cloud formation. Atmos. Chem. Phys. 7 (16), 4203–4227. http://dx.doi.org/10.5194/acp-7-4203-2007.

Keuken, M.P., Moerman, M., Zandveld, P., Henzing, J.S., Hoek, G., 2015. Total and size-resolved particle number and black carbon concentrations in urban areas near Schiphol airport (the Netherlands). Atmos. Environ. 104, 132–142. http://dx.doi.org/10.1016/j.atmosenv.2015.01.015.

Kinsey, J.S., Dong, Y., Williams, D.C., Logan, R., 2010. Physical characterization of the fine particle emissions from commercial aircraft engines during the Aircraft Particle Emissions eXperiment (APEX) 1–3. Atmos. Environ. 44 (17), 2147–2156. http://dx.doi.org/10.1016/j.atmosenv.2010.02.010.

Kinsey, J.S., Hays, M.D., Dong, Y., Williams, D.C., Logan, R., 2011. Chemical characterization of the fine particle emissions from commercial aircraft engines during the Aircraft Particle Emissions eXperiment (APEX) 1 to 3. Environ. Sci. Technol. 45 (8), 3415–3421. http://dx.doi.org/10.1021/es103880d.

Kolaitis, L.N., Bruynseels, F.J., Van Grieken, R.E., Andreae, M.O., 1989. Determination of methanesulfonic acid and non-sea-salt sulfate in single marine aerosol particles. Environ. Sci. Technol. 23 (2), 236–240. http://dx.doi.org/10.1021/es00179a018.

Lee, D.S., Fahey, D.W., Forster, P.M., Newton, P.J., Wit, R.C.N., Lim, L.L., Owen, B., Sausen, R., 2009. Aviation and global climate change in the 21st century. Atmos. Environ. 43, 3520–3537. http://dx.doi.org/10.1016/j.atmosenv.2009.04.024.

Liati, A., Brem, B.T., Durdina, L., Vögtli, M., Arroyo Rojas Dasilva, Y., Dimopoulos Eggenschwiler, P., Wang, J., 2014. Electron microscopic study of soot particulate matter emissions from aircraft turbine engines. Environ. Sci. Technol. 48 (18), 10975–10983. http://dx.doi.org/10.1021/es501809b.

Liu, D.-Y., Prather, K.A., Hering, S.V., 2000. Variations in the size and chemical composition of nitrate-containing particles in riverside, CA. Aerosol Sci. Technol. 33 (1–2), 71–86. http://dx.doi.org/10.1080/027868200410859.

Lobo, P., Durdina, L., Smallwood, G.J., Rindlisbacher, T., Siegerist, F., Black, E.A., Yu, Z., Mensah, A.A., Hagen, D.E., Miake-Lye, R.C., Thomson, K.A., Brem, B.T., Corbin, J.C., Abegglen, M., Sierau, B., Whitefield, P.D., Wang, J., 2015. Measurement of aircraft engine non-volatile pm emissions: results of the aviation – particle regulatory instrument demonstration experiment (A-PRIDE) 4 Campaign. Aerosol Sci. Technol. http://dx.doi.org/10.1080/02786826.2015.1047012.

Lobo, P., Hagen, D.E., Whitefield, P.D., Alofs, D.J., 2007. Physical characterization or aerosol emissions from a commercial gas turbine engine. J. Propuls. Power 23, 919–929. http://dx.doi.org/10.2514/1.26772.

Mauney, T., Adams, F., Sine, M.R., 1984. Carbonaceous particles in the atmosphere 1983 laser microprobe mass spectrometry of environmental soot particles. Sci. Total Environ. 36, 215–224. http://dx.doi.org/10.1016/0048-9697(84)90269-9.

Mazaheri, M., Bostrom, T.E., Johnson, G.R., Morawska, L., 2013. Composition and morphology of particle emissions from in-use aircraft during takeoff and landing. Environ. Sci. Technol. 47, 5235–5242. http://dx.doi.org/10.1021/es3046058.

Miller, R.A., 1997. Thermal barrier coatings for aircraft engines: history and directions. J. Therm. Spray Technol. 6 (1), 35–42. http://dx.doi.org/10.1007/BF02646310.

Neeft, J.P.A., Nijhuis, T.X., Smakman, E., Makkee, M., Moulijn, J.A., 1997. Kinetics of the oxidation of diesel soot. Fuel 76 (12), 1129–1136. http://dx.doi.org/10.1016/S0016-2361(97)00119-1.

Onasch, T.B., Jayne, J.T., Herndon, S., Worsnop, D.R., Miake-Lye, R.C., Mortimer, I.P., Anderson, B.E., 2009. Chemical properties of aircraft engine particulate exhaust emissions. J. Propuls. Power 25, 1121–1137. http://dx.doi.org/10.2514/1.36371.

Pagan, I., Costa, D.L., McGee, J.K., Richards, J.H., Dye, J.A., Dykstra, M.J., 2003. Metals mimic airway epithelial injury induced by in vitro exposure to Utah Valley ambient particulate matter extracts. J. Toxicol. Environ. Health Part A 66 (12), 1087–1112. http://dx.doi.org/10.1080/15287390390213908.

Park, K., Kittelson, D.B., Zachariah, M.R., McMurry, P.H., 2004. Measurement of inherent material density of nanoparticle agglomerates. J. Nanoparticle Res. 6, 267–272. http://dx.doi.org/10.1023/B: NANO.0000034657.71309.e6.

Pastor, S.H., Allen, J.O., Hughes, L.S., Bhave, P., Cass, G.R., Prather, K.A., 2003. Ambient single particle analysis in Riverside, California by aerosol time-of-flight mass spectrometry during the SCOS97-NARSTO. Atmos. Environ. 37 (Suppl. 2), 239–258. http://dx.doi.org/10.1016/S1352-2310(03)00393-5.

Petzold, A., Schröder, F.P., 1998. Jet engine exhaust aerosol characterization. Aerosol Sci. Technol. 28 (1), 62–76. http://dx.doi.org/10.1080/02786829808965512.

Qiu, C., Khalizov, A.F., Hogan, B., Petersen, E.L., Zhang, R., 2014. High sensitivity of diesel soot morphological and optical properties to combustion temperature in a shock tube. Environ. Sci. Technol. 48 (11), 6444–6452. http://dx.doi.org/10.1021/es405589d.

Rogers, F., Arnott, P., Zielinska, B., Sagebiel, J., Kelly, K.E., Wagner, D., Lighty, J.S., Sarofim, A.F., 2005. Real-time measurements of jet aircraft engine exhaust. J. Air Waste Manag. Assoc. 55, 583–593. http://dx.doi.org/10.1080/10473289.2005.10464651.

Rudich, Y., Donahue, N.M., Mentel, T.F., 2007. Aging of organic aerosol: bridging the gap between laboratory and field studies. Annu. Rev. Phys. Chem. 58, 321–352. http://dx.doi.org/10.1146/annurev.physchem.58.032806.104432.

SAE, 2004. Aerospace Information Report 5892: Nonvolatile Exhaust Particle Measurement Techniques.

SAE, 2010. Aerospace Information Report 6037: Aircraft Exhaust Nonvolatile Particle Matter Measurement Method Development.

SAE, 2013. Aerospace Information Report 6241: Procedure for the Continuous Sampling and Measurement of Non-volatile Particle Emissions from Aircraft Turbine Engines.

Schumann, U., 1996. On Conditions for Contrail Formation from Aircraft Exhausts. Meteorologische Zeitschrift/DLR, Inst. f. Physik der Atmosphäre, Report No. 44, 5, pp. 4–23.

Shapiro, M., Vainshtein, P., Dutcher, D., Emery, M., Stolzenburg, M., Kittelson, D.B., McMurry, P.H., 2012. Characterization of agglomerates by simultaneous measurement of mobility, vacuum aerodynamic diameter and mass. J. Aerosol Sci. 44, 24–45. http://dx.doi.org/10.1016/j.jaerosci.2011.08.004.

Silva, P.J., Carlin, R.A., Prather, K.A., 2000. Single particle analysis of suspended soil dust from Southern California. Atmos. Environ. 34 (11), 1811–1820. http://dx.doi.org/10.1016/S1352-2310(99)00338-6.

Silva, P.J., Prather, K.A., 2000. Interpretation of mass spectra from organic compounds in aerosol time-of-flight mass spectrometry. Anal. Chem. 72 (15), 3553–3562. http://dx.doi.org/10.1021/ac9910132.

Spencer, M.T., Prather, K.A., 2006. Using ATOFMS to determine OC/EC mass fractions in particles. Aerosol Sci. Technol. 40, 585–594. http://dx.doi.org/10.1080/02786820600729138.

Terzano, C., Di Stefano, F., Conti, V., Graziani, E., Petroianni, A., 2010. Air pollution ultrafine particles: toxicity beyond the lung. Eur. Rev. Med. Pharmacol. Sci. 14 (10), 809–821.

Timko, M.T., Onasch, T.B., Northway, M.J., Jayne, J.T., Canagaratna, M.R., Herndon, S.C., Wood, E.C., Miake-Lye, R.C., Knighton, W.B., 2010. Gas turbine engine emissions—Part II: chemical properties of particulate matter. J. Eng. Gas Turbines Power 132 (6). http://dx.doi.org/10.1115/1.4000132, 061505–061505.

Touri, L., Marchetti, H., Sari-Minodier, I., Molinari, N., Chanez, P., 2013. The airport atmospheric environment: respiratory health at work. Eur. Respir. Rev. 22 (128), 124–130. http://dx.doi.org/10.1183/09059180.00005712.

TSI, I., 2004. Series 3800 Aerosol Time-of-flight Mass Spectrometers with Aerodynamic Focusing Lens Technology (Shoreview, MN).

Vander Wal, R.L., Bryg, V.M., 2014. Chemistry Characterization of Jet Aircraft Engine Particulate by XPS: Results from APEX III.

Yim, S.H.L., Lee, G.L., Lee, I.H., Allroggen, F., Ashok, A., Caiazzo, F., Eastham, S.D., Malina, R., Barrett, S.R.H., 2015. Global, regional and local health impacts of civil aviation emissions. Environ. Res. Lett. 10, 034001. http://dx.doi.org/10.1088/1748-9326/10/3/034001.

Zhou, C., Penner, J.E., 2014. Aircraft soot indirect effect on large-scale cirrus clouds: is the indirect forcing by aircraft soot positive or negative? J. Geophys. Res. Atmos. 119 (19), 11,303–11,320. http://dx.doi.org/10.1002/2014JD021914.